# Performance and Stability Analyses of Rocket Thrust Chambers with Oxygen/Methane Propellants

James R. Hulka*
*Jacobs Engineering ESTS Group, Huntsville, AL, 35812*

Gregg W. Jones†
*NASA Marshall Space Flight Center, Huntsville, AL, 35812*

**Liquid rocket engines using oxygen and methane propellants are being considered by the National Aeronautics and Space Administration (NASA) for future in-space vehicles. This propellant combination has not been previously used in flight-qualified engine systems developed by NASA, so limited test data and analysis results are available at this stage of early development. As part of activities for the Propulsion and Cryogenic Advanced Development (PCAD) project funded under the Exploration Technology Development Program, the NASA Marshall Space Flight Center (MSFC) has been evaluating capability to model combustion performance and stability for oxygen and methane propellants. This activity has been proceeding for about two years and this paper is a summary of results to date. Hot-fire test results of oxygen/methane propellant rocket engine combustion devices for the modeling investigations have come from several sources, including multi-element injector tests with gaseous methane from the 1980s, single element tests with gaseous methane funded through the Constellation University Institutes Program, and multi-element injector tests with both gaseous and liquid methane conducted at the NASA MSFC funded by PCAD. For the latter, test results of both impinging and coaxial element injectors using liquid oxygen and liquid methane propellants are included. Configurations were modeled with two one-dimensional liquid rocket combustion analysis codes, the Rocket Combustor Interactive Design and Analysis code and the Coaxial Injector Combustion Model. Special effort was focused on how these codes can be used to model combustion and performance with oxygen/methane propellants *a priori*, and what anchoring or calibrating features need to be applied, improved or developed in the future. Low frequency combustion instability (chug) occurred, with frequencies ranging from 150 to 250 Hz, with several multi-element injectors with liquid/liquid propellants, and was modeled using techniques from Wenzel and Szuch. High-frequency combustion instability also occurred at the first tangential (1T) mode, at about 4500 Hz, with several multi-element injectors with liquid/liquid propellants. Analyses of the transverse mode instability were conducted by evaluating injector resonances and empirical methods developed by Hewitt.**

## Nomenclature

| | | |
|---|---|---|
| $B_A$ | = | droplet size constant used in CICM |
| $C_A$ | = | atomization constant used in CICM |
| $c^*$ | = | characteristic exhaust velocity, ft/sec |
| *d, D* | = | diameter, inches |
| $\overline{D}_j$ | = | mean droplet diameter used in CICM, microns |
| $E_m$ | = | Rupe mixing efficiency |
| *f* | = | frequency, Hz |
| *ID* | = | inner diameter, inches |
| *L* | = | length, inches |
| *L'* | = | geometrical chamber length (injector face to geometric throat), inches |

* Engineering Specialist, ER32, Mail Stop ER32, NASA MSFC, Senior Member AIAA.
† Aerospace Engineer, ER32, Mail Stop ER32, NASA MSFC, Member AIAA.

$L^*$ = characteristic chamber length, inches
$M_A$ = jet stripping rate used in CICM
*MR, O/F* = oxidizer-to-fuel mixture ratio
$P$ = pressure, psia
$r_m$ = mass median liquid droplet diameter, microns
$U_r$ = relative velocity, ft/sec
$Z$ = axial location, ft
$V$ = velocity, ft/sec
$\eta$ = efficiency
$\mu$ = absolute viscosity, lbm/ft-sec
$\rho$ = density, lbm/ft$^3$
$\sigma$ = surface tension, lbf/ft

Subscripts
*b* = barrel (cylindrical section)
*c* = chamber
*c** = characteristic exhaust velocity
*g* = gas
*ie* = injector end
$I_{sp}$ = specific impulse
*j* = jet
*L* = liquid
*m* = measured
*mix* = mixing
*vap* = vaporization

## I. Introduction

NASA has been considering use of oxygen and methane propellants for propulsion of future space exploration vehicles for several years.[1,2] Unfortunately, engine systems with oxygen and methane propellants have never been previously certified or flight-qualified by NASA, so test data and analysis results are limited at this stage of preparation. NASA has funded two efforts in the past 40 years for thrust chamber development with oxygen/methane propellants. During the late 1970s through the 1980s, NASA examined oxygen/methane propellants for high-chamber pressure boost phase engine applications. Methane as a booster engine propellant was considered a compromise between the density of a hydrocarbon like kerosene and the performance of hydrogen. Thrust chamber development activities included the design, development and test of shear and swirl coaxial element injectors.[3-7] Since the methane was to be used as combustion chamber and nozzle coolant, it was delivered to the injectors in gaseous form. High performance (>98% $\eta_{C^*}$) was achieved, although high-frequency combustion instability was observed with some configurations.[7] The liquid oxygen ($LO_2$), gaseous methane ($gCH_4$) propellant conditions were recently revisited in a hot-fire demonstration at the NASA Marshall Space Flight Center (MSFC), with similar performance results.[8] Also, as part of university-level research investigations funded by the NASA Constellation University Institutes Program (CUIP), a single-element thrust chamber was tested with shear and swirl coax element injectors, which included measurement of local heat flux.[9]

More recently, NASA has considered oxygen/methane propellants for in-space rather than booster applications. Spacecraft propulsion systems using oxygen/methane propellants have several advantages over systems that use hypergolic propellants, including reduction in spacecraft mass due to higher engine specific impulse, the ability to use common oxygen tanks for other subsystems (such as life support), and the possibility to produce these propellants *in situ*, thus reducing the need to carry them to extraterrestrial surfaces.[1] In addition, ground crews and astronauts can operate in inherently safer environments when manipulating oxygen and methane propellant systems compared to hypergolic propellant systems.[1] For these low to moderate chamber pressure engines, where turbopump-cycles are less likely to be used, the methane is less likely to be used as thrust chamber coolant, and thus would be delivered to the injector in cryogenic liquid form ($LCH_4$).[1,10] Since design, analysis, and experimental studies with $LCH_4$ to date are even less extensive than with $gCH_4$, NASA has recently funded, through the Propulsion and Cryogenic Advanced Development (PCAD) project under the Exploration Technology Development Program at the NASA Glenn Research Center (GRC), several programs for $LO_2/LCH_4$ propellant thrust chamber development. Four separate commercial thrust chamber programs have been or are being conducted,[10-14] while

NASA has conducted additional in-house development activities at the MSFC.[15-18] Performance with $LCH_4$ injectors has generally been moderate ($\eta_{C*}$~93-96%) with instances of excessively noisy combustion, low frequency combustion instability (chug), and high-frequency transverse mode combustion instability.

As part of these activities, the NASA MSFC has also been funded by PCAD to evaluate the liquid propellant rocket engine analysis tools for combustion of oxygen and methane propellants, especially combustor performance and combustion stability. The outcome of these evaluations will be an assessment of the readiness to conduct future combustion analyses with these propellants, along with the definition of anchoring techniques and recommendations of code improvements where applicable. The current one-dimensional combustion and performance codes and the combustion Computational Fluid Dynamic (CFD) analysis codes were originally developed largely for other propellants and have never been adequately validated for use with oxygen and methane propellants.

The performance evaluation task at NASA MSFC was divided into 3 subtasks: 1) selection of appropriate modeling data sets, 2) evaluation of one-dimensional combustion and performance analysis codes, and 3) evaluation of a combustion CFD code. The first subtask gathered existing methane data and selected appropriate data sets that can be used to most effectively evaluate the analysis tools. In the second subtask, several of these configurations were modeled using the one-dimensional analysis codes Rocket Combustor Interactive Design and Analysis (ROCCID)[19] and the Coaxial Injector Combustion Model (CICM).[20] For most of the selected cases, anchoring or calibrating values of inputs in the analyses codes were varied to evaluate sensitivities of the analysis techniques and to determine the best anchoring values for future analyses. In the third subtask, several of the single-element chamber configurations have been and are being analyzed with Loci-CHEM, a CFD code under development at the NASA MSFC.[21]

The combustion stability modeling task was a more recent addition due to the growing realization of potential combustion instability issues with oxygen and methane propellants, especially with liquid methane. The effort has focused to date on evaluation and explanation of the NASA MSFC in-house test results, some of which is reported in this paper, but is planned to expand to the contractor programs in the future.

This paper describes the results of the combustion stability and one-dimensional performance analyses conducted to date on several hardware configurations tested with gaseous and liquid methane. Generally, descriptions of the hardware are not provided and the reader is encouraged to examine the cited references for this information. Also, combustion CFD results are not reported in this paper, but results of ongoing CFD analyses are expected to be reported in future papers.

## II. Liquid Oxygen and Gaseous Methane

Liquid oxygen and gaseous methane combustors were investigated by NASA in the past and have undergone more development than combustors with liquid methane. The use of gaseous methane in the injector provides the potential for high performance, while combustion instability has occurred in only one instance. Because the propellant conditions are liquid and gas, the coaxial element geometry, with the liquid injected in either shear or swirl form, is preferred, which brings to bear decades of development from oxygen/hydrogen injector systems.

### A. Performance

Tests of single-element injectors with shear and swirl coaxial elements and liquid oxygen/gaseous methane propellants were conducted at the Pennsylvania State University funded by the NASA CUIP.[9] The original purpose of these tests was to measure profiles of circumferential and axial local heat flux, similar to results gathered for coaxial elements with liquid oxygen/gaseous hydrogen propellants.[22,23,24] These heat flux data may also be used to examine the axial profile of energy release rate, since the energy release in the single element injector is likely to be similar to the heat flux profile. The overall $\eta_{c*}$ can also be measured and compared to calculations. Injector geometry and test data for the single-element hardware are summarized in Table I. For all these tests, $D_c$ was 1.0", $L_c$ was 14.49" with $L_b$ of 14.00", and contraction ratio was 5.38.

A comparison of performance for various element types is shown in Fig. 1. Note that $\eta_{c*}$ for the single element experiments were not reported in Ref. [9], but have been calculated for the current analyses. The $\eta_{c*}$ shown in Fig. 1 do not include heat loss to the chamber, which can provide a substantial increase to the efficiency, on the order of 2-4%. Thus, the measured $c^*$ without heat loss is likely incorrect since the performance is already approaching 100%. However, since all tests were run in the same facility, in close succession and with the same measurement system, the values shown in Fig. 1 are believed to be representative and reasonable indicators of the differences between the element types.

Table I. Single-element geometry and test data from NASA CUIP task at The Pennsylvania State University.[9]

| Case Number | | 9 | 10 | 11 | 1 | 12 | 2 | 3 | 4 |
|---|---|---|---|---|---|---|---|---|---|
| Coaxial Element Type | | Shear | Shear | Shear | Shear | Shear | Shear | Shear | Swirl |
| **OXIDIZER** | | | | | | | | | |
| post characteristics | -- | Recessed | Recessed | Recessed | Recessed | Recessed | Flush | Recessed | Flush |
| metering orifice ID (1) | in. | 0.092 | 0.092 | 0.092 | 0.092 | 0.092 | 0.117 | 0.117 | 3 x 0.020 x 0.332 |
| post exit ID | in. | 0.225 | 0.225 | 0.225 | 0.225 | 0.225 | 0.156 | 0.156 | 0.244 |
| exit taper angle | deg. | 5.8 | 5.8 | 5.8 | 5.8 | 5.8 | 0 | 0 | 0 |
| post exit thickness | in. | 0.015 | 0.015 | 0.015 | 0.015 | 0.015 | 0.020 | 0.020 | 0.020 |
| post length | in. | 3.775 | 3.775 | 3.775 | 3.775 | 3.775 | 1.875 | 1.875 | 2.225 |
| post recess | in. | 0.225 | 0.225 | 0.225 | 0.225 | 0.225 | 0 | 0.156 | 0 |
| **FUEL** | | | | | | | | | |
| annulus length | in. | 0.500 | 0.500 | 0.500 | 0.500 | 0.500 | 0.275 | 0.275 | 0.100 |
| gap width | in. | 0.024 | 0.024 | 0.024 | 0.024 | 0.024 | 0.029 | 0.029 | 0.020 |
| **TEST DATA** | | | | | | | | | |
| Test Number | -- | 15 | 23 | 27 | 20 | 14 | 11 | 51 | 42 |
| chamber pressure | psia | 291 | 595 | 795 | 1006 | 1199 | 984 | 1006 | 1016 |
| mixture ratio | -- | 2.84 | 2.98 | 3.00 | 3.00 | 2.99 | 3.09 | 3.00 | 3.00 |
| fuel manifold temperature | R | 510 | 515 | 515 | 516 | 509 | 515 | 512 | 518 |
| oxidizer flowrate/element | lbm/sec | 0.17 | 0.35 | 0.47 | 0.59 | 0.70 | 0.60 | 0.59 | 0.58 |
| $\eta_{C^*}$ (2) | % | (94.8) | (96.4) | (96.6) | (97.1) | (96.2) | (94.1) | (97.0) | (98.4) |

Notes:
(1) swirl coaxial metering is # slots x slot width x slot height
(2) PSU CUIP performance are estimates without heat loss to combustion chamber

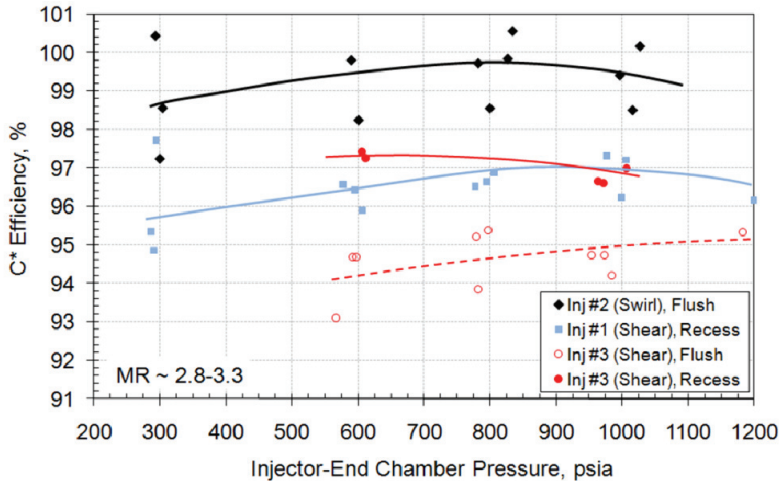


Figure 1. Relative performance of single-element injectors from Ref. [9]. Note heat loss is not included.

Configurations listed in Table I were modeled using the one-dimensional analysis codes ROCCID[19] and CICM.[20] The ROCCID code was capable of analyzing both elements. CICM is currently capable of analyzing only shear coaxial injection elements with liquid propellant in the center jet and gaseous propellant in the annulus.

Initial modeling iterations were conducted using pre-defined calibrating parameters. For the ROCCID code, such critical parameters include atomization lengths and droplet sizes, which can be selected from a list of several model-provided analytical or empirical calculations (or defined directly by the user or modified in the CONTROL file).[19] For CICM, four critical parameters are available for calibration: the atomization coefficient $C_A$ in the cup and the chamber for calculation of the jet stripping rate $M_A$, shown in Eqn. (1), and the droplet size production coefficient $B_A$ in the cup and the chamber for the calculation of the mean droplet size $\overline{\mathbf{D}}_j$, shown in Eqn. (2).[20] Values for these four parameters are currently only available for oxygen/hydrogen propellants.[20] A procedure that can be used to recalculate these parameters for oxygen/methane propellants is described in Ref. [20]. In the current model exercises, these parameters were varied to determine sensitivities of the analysis techniques and determine whether other values could best represent the test data.

$$M_A = C_A \left[ \frac{\mu_j (\rho_g U_r^2)^2}{\sigma_j / \rho_j} \right]^{1/3} \pi D_j (\Delta Z) \qquad (1)$$

Atomization Coefficient

$$\overline{D}_j = B_A \left[ \frac{\mu_j (\sigma_j / \rho_j)^{1/2}}{\rho_g U_r^2} \right]^{2/3} \qquad (2)$$

Drop Size Coefficient

For combustion analyses with ROCCID and CICM, injector mixing plays a key role that is often misunderstood. In the distributed energy release calculation procedures described in the JANNAF performance methodology,[25] as used in these models, the injection process is treated separately from the combustion process, which means that mass and mixture ratio distributions from the injector are defined before combustion is initiated. The part of the thrust chamber energy release efficiency associated with mixing loss, $\eta_{mix}$, is thus defined in the JANNAF performance methodology as the product of several independent factors, including the injector inter-element mixing efficiency, and the global mass and mixture ratio bias, which can be intentional (such as mass or mixture ratio variations across the injector face for combustion stabilization or near the chamber wall for wall compatibility), or unintentional (mass and mixture ratio variations across the injector face as a result of maldistributions from manifolding, element geometrical tolerances, etc.). In ROCCID, such injector face mass and mixture ratio biases can be included by the use of the two-zone (core and barrier), four-streamtube (core, barrier, baffle, and fuel film coolant) inputs.[19] In CICM, these zone biases must be calculated with independent runs and mass weighted outside the program, as suggested by Refs. [20] and [25]. However, neither program provides a completely model-defined calculation of the inter-element mixing efficiency. In the ROCCID model, an *inter*-element or overall injector mixing efficiency is defined by the user. This *inter*-element mixing efficiency can be calculated from *intra*-element – or single element – Rupe mixing efficiency,[26] or $E_m$, using techniques developed by Ito and Calhoon[25] combined with methods from the Liquid Injection Spray Pattern (LISP) calculation[28] or from Nurick.[29] No mixing calculations are included implicitly in CICM, which essentially calculates only the vaporization efficiency of the single element streamtube, which for single element type patterns can be assumed to be the vaporization efficiency of the thrust chamber, $\eta_{vap}$, as defined in the JANNAF performance methodology. The overall thrust chamber energy release efficiency (the product of $\eta_{mix}$ and $\eta_{vap}$) is provided in the ROCCID code, but must be calculated independently when using CICM.

1. *Single Element Cases – Shear Coax*

Modeling of the single-element shear coaxial element injector data showed how energy release rate ($\eta_{c*}$ or $\eta_{Isp}$) profiles, compared to axial and circumferential local heat flux profiles. The intra-element $E_m$ for the shear coaxial element cases were derived from a cold flow correlation developed by Burick,[30] which is reproduced in Fig. 2. For this correlation, $E_m$ was measured 5 inches from the injector face with a two-phase deceleration probe in a backpressure chamber, with water and air simulants for oxidizer and fuel, respectively.[30] Note that for most of the $LO_2/gCH_4$ element conditions, the correlation in Fig. 2 is out of range, as indicated.

A ROCCID calculation for Case 1 from Table I using an input $E_m$ of 83.5% and the internal submodel selection of DROPMIX droplet size parameters is shown in Fig. 3. For these input conditions, the predicted $\eta_{c*}$ matches the measured $\eta_{c*}$ and all the energy release loss is from mixing and none is from vaporization. Note that for Case 1 element operating conditions, the Burick correlation for $E_m$ is out of range. Extrapolating the Burick correlation to Case 1 conditions suggests an $E_m$ of about 81%, which would underpredict the measured $\eta_{c*}$ by about 0.7%.

In the single-element experiments, axial and circumferential local heat flux profiles were measured,[9] which may be considered a reasonable representation of the energy release rate. Figure 4 shows a 30% increase in droplet size from the DROPMIX submodel improves the match of the $\eta_{c*}$ profile to the heat flux profile and still allows a match of measured and calculated $\eta_{c*}$. Further increases in droplet size result in a vaporization efficiency less than 100% and a mismatch between measured and calculated $\eta_{c*}$ unless $E_m$ is also increased.

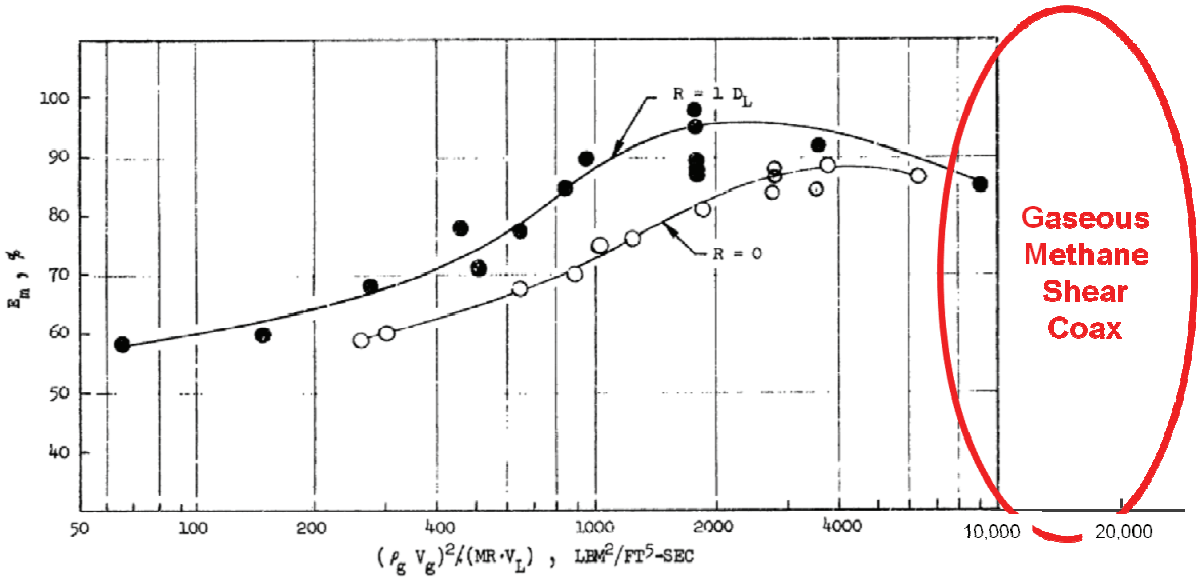


Figure 2. Correlation of cold flow single-element shear coax injector element Rupe mixing efficiency ($E_m$), from Burick,[30] extended to $LO_2/gCH_4$. Solid data points – oxidizer post recess of one orifice diameter. Open data points – no oxidizer post recess.

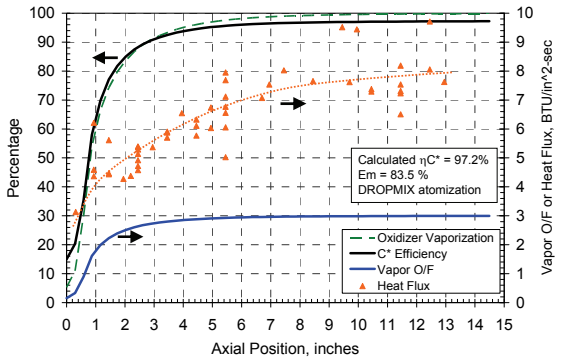


Figure 3. ROCCID analysis of single element recessed shear coax (Case 1).

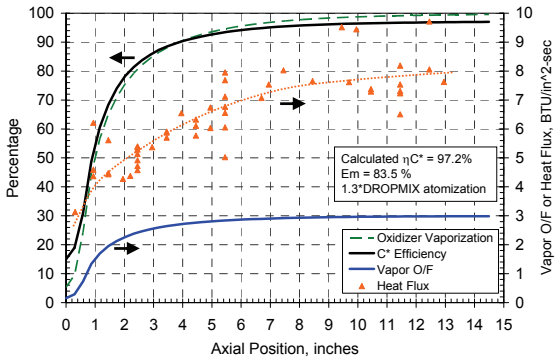


Figure 4. ROCCID analysis of single element recessed shear coax (Case 1) with increased droplet size.

Similar calculations with ROCCID for a smaller element without and with a cup recess are shown in Figs. 5 and 6, respectively. For Case 2 from Table I, the lack of the recessed oxidizer post ("cup") significantly decreased measured $\eta_{c*}$ as well as heat flux near the injector face. The Burick correlation of $E_m$ for non-recessed shear coaxial element is within the range of Case 2 conditions, and using the predicted $E_m$ of 83% resulted in the requirement to increase the DROPMIX droplet size by a factor of 2.2, as shown in Fig. 5. The mixing loss was about 2.5% $\Delta\eta_{c*}$, and the vaporization loss was about 3.5% $\Delta\eta_{c*}$. For Case 3 from Table I, the same element but with a recessed oxidizer post, the Burick correlation of $E_m$ for recessed shear coaxial element is also within the range of Case 3 conditions, and the predicted $E_m$ of 84% and the 1.3 factor on DROPMIX used for Case 1 compares favorably with measured $\eta_{c*}$ and heat flux profiles, as shown in Fig. 6. Use of the anchoring parameters for Case 3 compare very well with use of the anchoring parameters for Case 1, even though Case 3 has a smaller element and about half the fuel-to-oxidizer injection velocity ratio. However, the Burick parameter to predict $E_m$ is about the same, which suggests that the Burick correlation provides a reasonable means to predict mixing for recessed shear coaxial elements when in range of the correlation.

Off-nominal operating conditions for the recessed single-element shear coaxial injector of the single-element PSU testing, shown as Cases 9-12 in Table I, were next evaluated. The effect of throttling on $\eta_{c*}$ for this and the other injectors from the single-element test program was shown in Fig. 1. For the recessed shear coax design represented in Cases 9-12, at a *MR* of 3.0, the performance appears to peak at a $P_c$ of 1000 psia.

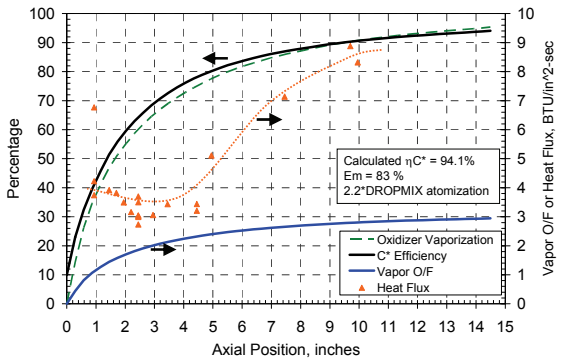


Figure 5. ROCCID analysis of single element non-recessed shear coax (Case 2).

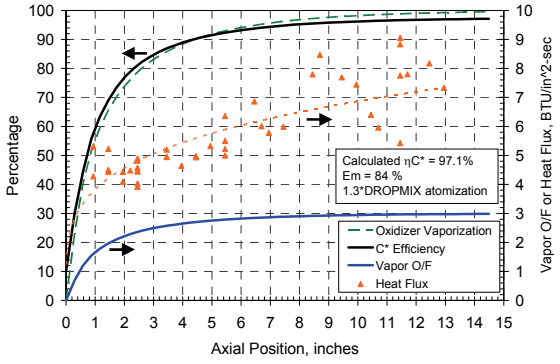


Figure 6. ROCCID analysis of recessed single element shear coax (Case 3).

The results of modeling a low-$P_c$ single-element recessed shear coax case with ROCCID are shown in Fig. 7. For this case, because the fuel density is lower, the $E_m$ calculated from Burick is in the range of the correlation but high – about 89% – and approaching the maximum. However, atomization quality has worsened, so the improvement in mixing efficiency is offset by a decrease in vaporization efficiency. Still, a combination of an $E_m$ of 89% and a 30% increase to the droplet size calculated by the DROPMIX program significantly overpredicts the performance. The performance mismatch can be corrected by using a 2.4 factor increase in droplet size with the $E_m$ of 89%, as shown in Fig. 7(a), or an $E_m$ of 79.5% and the 1.3 factor increase to the droplet size, as shown in Fig. 7(b). The former appears a better match to the heat flux data profile.

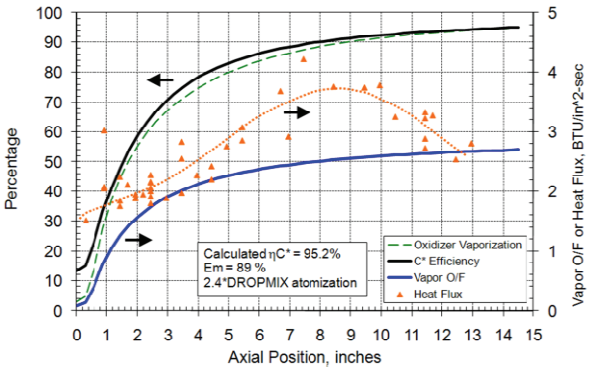


(a) $E_m$=89% and 2.4x increase in dropsize

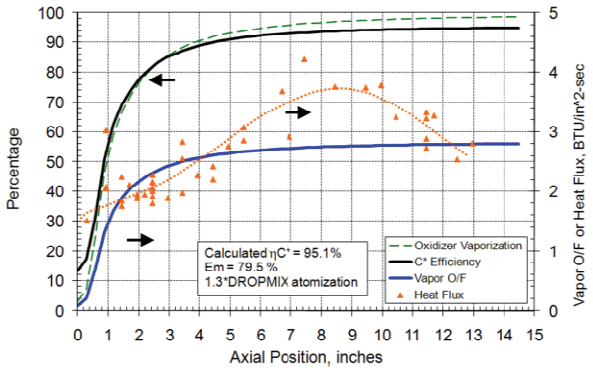


(b) $E_m$=79.5% and 1.3x increase in dropsize

Figure 7. ROCCID analysis of single-element recessed shear coax injector at $P_c$~300 psia (Case 9).

The results of modeling a high-$P_c$ single-element recessed shear coax case (Case 12) with ROCCID are shown in Fig. 8. For this case, because the fuel density is much higher, an $E_m$ from Burick is considerably out of range of the correlation; an estimate for $E_m$ is 76%. Thus, mixing efficiency is considerably decreased from the low-$P_c$ case, although the $\eta_{c*}$ loss has been partially offset by an improvement in atomization quality and increase in vaporization efficiency. Still, with use of an $E_m$ of 76% the performance is underpredicted by 1.5% even with 100% vaporization efficiency. Use of an $E_m$ of 81% allows the calculation to match the measured data.

Thus, modeling off-nominal conditions of the single-element recessed shear coaxial injector with ROCCID suggests that using the Burick correlation for $E_m$ – either reading directly from the plot or extrapolating – may be erroneous, especially at low-$P_c$ conditions. Using a 30% increase to the droplet size calculated by the DROPMIX program, $E_m$ is required to be about the same value – ~ 82% – for all cases. A re-evaluation of the mixing efficiency from Burick for elements with dense fuels is recommended.

CICM is currently capable of analyzing only shear coaxial injection elements with liquid propellant in the center jet and gaseous propellant in the annulus, and has only been validated with liquid oxygen and gaseous hydrogen propellants.[20] These restrictions makes the model less appealing for developing capability to analyze $LO_2/LCH_4$, but

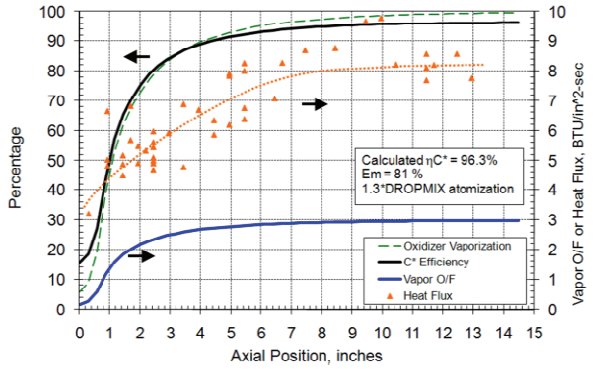


Figure 8. ROCCID analysis of single-element recessed shear coax injector at $P_c$~1200 psia (Case 12).

it was included in this analysis development program since CICM is the industry standard for liquid/gas shear coaxial element calculations in JANNAF,[25] and its calculation procedure for atomization may be used in future models. Note that as discussed earlier, CICM does not calculate or include an intra-element mixing non-uniformity, such as shown in Fig. 2, so that the mixing loss must be included either through averaging of several calculations at different mixture ratios, or an *ad hoc* addition of a mixing efficiency to the CICM-calculated vaporization efficiency. Such mixing losses were not included in the results presented here.

The use of CICM for oxygen and methane calculations requires new propellant and combustion property data, and new parameters for the semi-empirical atomization correlations. The thermodynamic property data required for $CH_4$ propellant and $LO_2/CH_4$ combustion have been developed during this program. Atomization parameters are currently only validated in available documentation for oxygen/hydrogen propellants with shear coaxial element geometries similar to those in the J-2 injector.[20] Three methods to recalculate these parameters for other propellants or radically different shear coaxial element geometries, which all use the cup pressure drop in the calculations, are described in the CICM User's Manual.[20] Unfortunately, the methods were found to be inapplicable to most of the single-element $LO_2/gCH_4$ experimental test cases since the cup pressure drops were found to be practically zero, which is not surprising given that reaction rates for $LO_2/gCH_4$ propellants are considerably slower than for $LO_2/gH_2$ propellants. The best opportunity to determine cup pressure drops was with the elements in Cases 2 and 3, using both recessed and flush configurations. Unfortunately, even for this case, the cup pressure drop could not be determined for several cases of $P_c$ and *MR*. Thus, the recommended methods in Ref. [20] to determine new atomization parameters could not be used.

Consequently, to determine correlating parameters for the $LO_2/gCH_4$ propellants, all of the parameters were varied individually, starting with the values in the CICM user manual for $LO_2/gH_2$ propellants. Two parameters were found that showed the strongest influence and provided the most correct trends – chamber droplet formation size parameter BSPRC, and chamber liquid jet stripping rate CSPRC. These two parameters were subsequently varied together, in an attempt to determine the best match of the heat flux profile and the $\eta_{C^*}$ data from all the appropriate single-element test cases. All of the cases were then re-examined with the best correlating parameters.

The initial calculation using manual-suggested inputs for $B_A$ and $C_A$ in the cup and the chamber from $LO_2/gH_2$ propellants is shown in Fig. 9. Comparing the heat flux profile and the $\eta_{c^*}$ profile calculated with these parameters shows the energy release near the injector (the first 2 or 3 inches of the combustion chamber) may be underpredicted, while the final calculated $\eta_{c^*}$ significantly underpredicts the measured $\eta_{c^*}$ even though the result is from vaporization losses only and does not include mixing losses as found in a parameter such as $E_m$. Use of the $B_A$ and $C_A$ in the cup and the chamber from the manual are obviously not valid with oxygen and methane propellants.

Selection of better values for atomization parameters was subsequently an exercise trading improving the atomization rates and hence increasing the vaporization rates of the cases with under-predicted performance, and not significantly altering the already higher performing cases. A prediction with atomization parameters revised for $LO_2/gCH_4$ is also shown in Fig. 9, which indicates a more rapid rise in energy release rate near the injector. The chamber liquid jet stripping parameter had the largest effect on the initial vaporization rate near the head end of the chamber, while the chamber droplet formation size parameter was used to reduce the vaporization rate in the far field. However, while there was a large change in the profiles for the element in Case 1, there was only a minor change to the profile for the smaller geometry element in Case 3. The revised atomization parameters provided similar modeling comparisons for most of the cases analyzed.

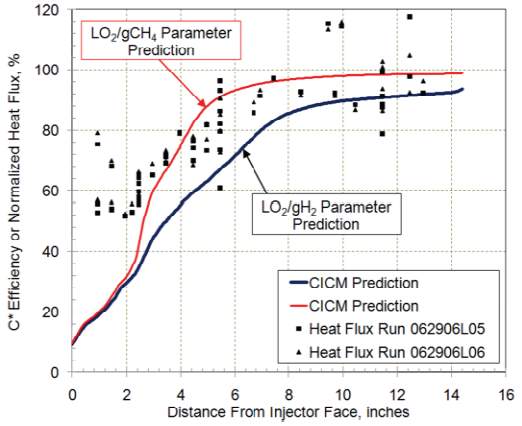


Figure 9. Comparison of CICM atomization parameters to match axial $\eta_{c*}$ profiles to axial heat flux data. Case 1 at $P_c$~1000 psia.

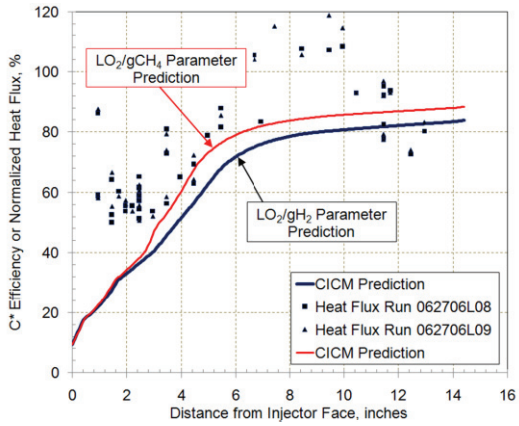


Figure 10. CICM $LO_2/gCH_4$ atomization parameters underpredict $\eta_{c*}$ for Case 9 at $P_c$~300 psia.

However, using the revised atomization parameters for low $P_c$~300 psia (Case 9 in Table I), CICM significantly underpredicted $\eta_{C*}$, as shown in Fig. 10. One possible reason for this error is that oxygen is subcritical at this $P_c$ compared to other tests examined. Correlation parameters from conditions with much lower (subcritical) chamber pressures are likely to be different than those developed for high chamber pressures. Second, this $P_c$ is throttled to 30% of the nominal design point of this injector element, providing significantly off-nominal operating conditions.

2. *Single Element Cases – Swirl Coax*

For the swirl coaxial single-element injector, Case 4 from Table I, several inputs had to be modified for the measured $\eta_{c*}$ and the axial heat flux profiles to match. Results from unmodified calculations are shown in Fig. 11. The $E_m$ for the swirl coaxial elements were estimated from data in Hulka et.al.,[31] for which $E_m$ was measured 5 to 6 inches from the injector face with a patternator at atmospheric pressure, with water and sucrose simulants for oxidizer and fuel, respectively. Swirl coaxial element geometries were varied at constant oxidizer-to-fuel momentum ratios of about 3, and found the oxidizer free swirl angle to be most influential on $E_m$.[31] Figure 11 shows the $\eta_{c*}$ was overpredicted by 1.2%, while the start of combustion is delayed too far downstream due to a significant overprediction of primary atomization lengths. To improve the match to measured parameters, the program-calculated atomization length had to be reduced by a factor of 10, the droplet size from the AEROJET submodel increased by a factor of 2.7, and the $E_m$ estimated from Ref. [31] reduced from 94% to 88%. The results of these modifications are shown in Fig. 12. A large change in $E_m$ is not surprising given the differences in oxidizer-to-fuel momentum ratio for Case 4 (about 0.3) from Ref. [31] (about 3). The significant alterations from calculated atomization parameters (primary atomization lengths, droplet diameters used in vaporization calculations) suggest that the atomization model does not adequately represent the mechanisms of the swirled oxidizer atomization.

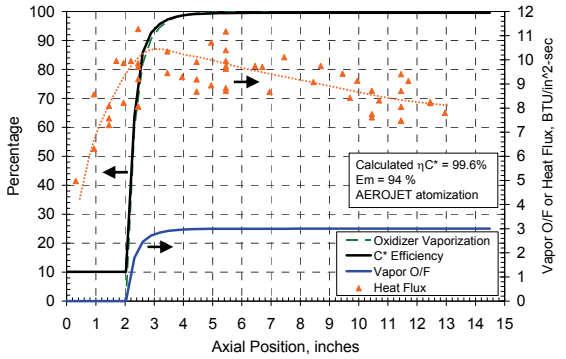


Figure 11. ROCCID analysis of single-element swirl coax (Case 4), without modifications.

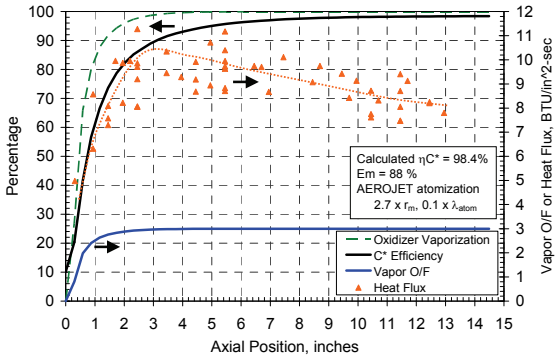


Figure 12. ROCCID analysis of single-element swirl coax (Case 4), with modifications.

3. *Multielement Cases*

Calculations with ROCCID for a multielement liquid/gas shear coaxial injector[7] are shown in Fig. 13, using the same 1.3 factor on DROPMIX droplet size from the previous calculations with recessed shear coaxial elements, shown in Figs. 4 and 6. However, these conditions are far outside the range of the Burick correlation of $E_m$ for recessed shear coaxial elements shown in Fig. 2. An extrapolation of the Burick correlation to these conditions would result in a completely unrealistic $E_m$, so a prediction of $E_m$ could not be made. An $E_m$ of 83.6% was used to match measured $\eta_{c*}$. Clearly, if shear coaxial injection elements will be used for future injectors using liquid oxygen and gaseous methane propellants, the Burick correlation for $E_m$ should be extended to include typical ranges of values for those propellants. While there were no heat flux data for this element, CICM analysis with the $LO_2/CH_4$ correlating parameters provides a reasonable match with the ROCCID results, as shown in Fig. 14.

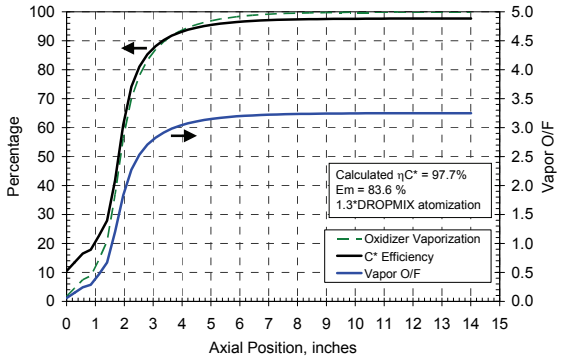


Figure 13. ROCCID analysis of multi-element shear coax injector.

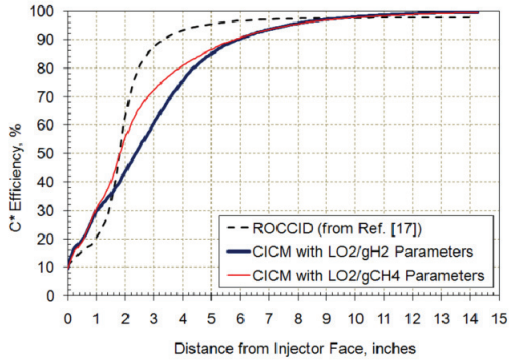


Figure 14. Comparison of CICM and ROCCID $\eta_{c*}$ profiles for multi-element shear coaxial injector.

## B. Combustion Stability

With one exception, combustion instability with $LO_2$ and $gCH_4$ propellants has been relatively absent. In one 82-element shear coaxial element injector in a 5.66" combustion chamber diameter at booster-level $P_c$~1500 psia to 2000 psia, injection-coupled combustion instability occurred as a result of coupling between the "organ-pipe" resonance of the oxidizer element tube and the first tangential (1T) mode of the combustion chamber.[7] The comparison of organ pipe responses for injectors with different length injector oxidizer tubes and the combustion chamber response is shown in Fig. 15. Further details and discussion of the injection-coupled analyses of this instability are provided in Refs. [7] and [32].

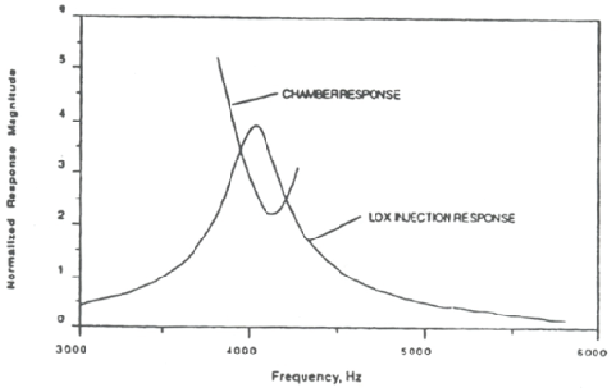


(a) Injector configuration that exhibited spontaneous 1T mode combustion instability

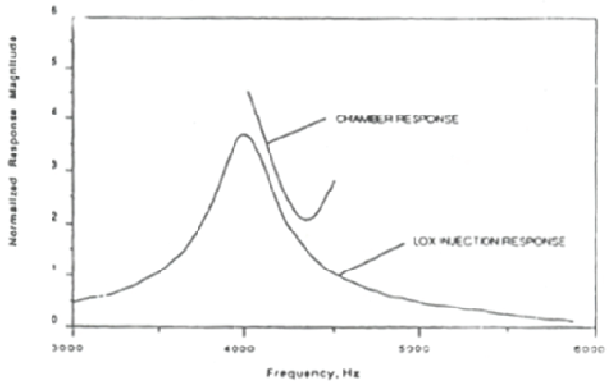


(b) Injector configuration that was stable

Figure 15. Comparison of calculated combustion chamber and oxidizer injector injection responses for two shear coaxial element injectors with different oxidizer post lengths.[7]

### C. Regenerative Chamber Heat Transfer and Cooling

In engine cycles with regeneratively cooled combustion chambers or nozzles, the methane delivered to the injector is in gaseous form because of heat addition as a coolant. Development of such chambers will require further research and development into how subcritical methane changes phase in the coolant circuits, and especially how that process couples to other engine dynamics and becomes a system oscillation. Additional development of the methane combustion chamber cooling design features is also needed. NASA is currently conducting work in these areas, with plans to report in future papers.

## III. Liquid Oxygen and Liquid Methane

The use of pressure-fed engine systems, such as expected for in-space applications, usually means that combustion chamber or nozzle regenerative cooling is not likely or not feasible, so the methane will be delivered to the injector in liquid form. With both propellants now in liquid form, the impinging element geometry, from storable propellant or oxygen/RP-1 history, can be employed. Reasonable combustion efficiencies have been demonstrated along with stable combustion, although modeling has suggested that higher efficiencies can be achieved. However, because the fuel density is not as high as MMH or RP-1, the coaxial element geometry can also be considered. In-house NASA MSFC testing with swirl coaxial element injectors in 5.66" diameter combustor hardware has demonstrated high efficiencies in relatively long combustion chambers (exceeding 20 inches in length), although combustion instability, at both low and high frequencies, has occurred with several configurations.[15,17,18] The coaxial element used in these studies swirled the $LO_2$ in the center post and injected the $LCH_4$ axially through the outer annulus, as shown in Fig. 16. The oxidizer metering orifice, the fuel sleeve, and the face nut were modular and replaceable allowing for variations of oxidizer and fuel metering area to be tested. The tangential entry orifices for the oxidizer swirl were slots formed by electro-discharge machining.

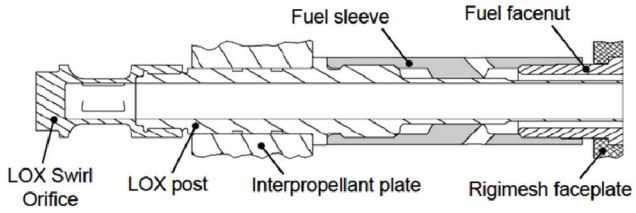


Figure 16. Typical swirl coaxial injector element details.[15,17,18]

### A. Performance

Performance calculations of tests using $LO_2/LCH_4$ propellants with a NASA MSFC in-house multi-element like-on-like (LOL) doublet impinging element injector[15] were conducted with ROCCID. $E_m$ for this element type can be predicted from several sources, including Refs. [28], [29], or [33]. Using the like-impinging doublet correlation from Ref. [29] with no edge-on-edge offset and the design cant angle, an $E_m$ of 77% is predicted. Using this $E_m$ and the DROPMIX atomization parameters, the initial calculation is shown in Fig. 17. The predicted $\eta_{c*}$ of 95.4% in the initial model without modifications provided an excellent match to the measured $\eta_{c*}$ of 95.6%.

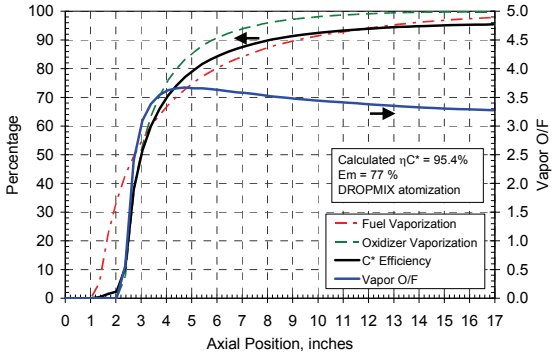


Figure 17. ROCCID analysis of multi-element paired like-on-like injector with $LO_2/LCH_4$ propellants.

The good match of ROCCID predictions to measured performance with this injector concept suggests several avenues to increase performance. First, several aspects of the paired doublet geometry can be altered to increase the $E_m$, e.g., an increase in the cant angle. Within the range of the correlation from Ref. [29], $E_m$ can be increased from 77% to 84% and $\eta_{c*}$ can improve up to 2%. References [28] and [29] also suggest impingement angles and momentum ratios are not optimum for performance. Second, the orifice dimensions could be reduced and the number of elements increased, according to LOL element combustion stability guidelines such as from the Hewitt Stability Correlation,[34,35] and still meet combustion stability margin requirements, especially if baffles and/or head-end acoustic resonator cavities are included. While the tested element packaging had an element pattern density similar to several development and flight $LO_2$/RP-1 LOL element injector patterns, higher performance (~99% $\eta_{c*}$) has been achieved in drilled-orifice element patterns with 40% more elements-per-area, such as the Titan I second stage engine. Higher element density patterns can also be fabricated with other means than conventionally drilled plates, such as platelets or micro-orifices. The use of an improved $E_m$ and more injection elements suggests the performance of this injector can be significantly improved. On the other hand, a wall compatible element or some level of barrier cooling would subsequently be required which would reduce performance.

Calculations of a test from a NASA MSFC in-house 28-element swirl coaxial element injector[15,17] are shown in Fig. 18. To be able to perform these analyses, the ROCCID code was modified in 2008 to include the capability to analyze a swirl coaxial injector element with liquid flow from both circuits.[19] In Fig. 18, the uni-element $E_m$ ~ 94% was estimated from Hulka et.al.,[31] a cold flow mixing study conducted with liquid/liquid simulants. However, the new atomization submodel provided unreasonably large atomization lengths and droplet sizes that resulted in greatly underpredicted $\eta_{c*}$. For the predictions to match the test data, considerable reductions were required in atomization length (factor of 0.2) and droplet size from the AEROJET model (factor of 0.17), similar to alterations shown earlier from the $LO_2$/$gCH_4$ cases. A calculation using the same atomization factors, at similar $P_c$ and *MR* but with a longer combustion chamber, is shown in Fig. 19. Since the measureable increase in $\eta_{c*}$ from the extra 4" of combustion chamber length was predicted reasonably well, the injector is shown to be vaporization limited, and the droplet size parameters used in the calculations are probably representative. Note that the $LO_2$ vaporization efficiency is lower than the $LCH_4$ vaporization efficiency, with both contributing to performance loss in the *L'*=20" chamber. At *L'*=24", the $LCH_4$ vaporization is practically complete, while the $LO_2$ vaporization is still limiting performance.

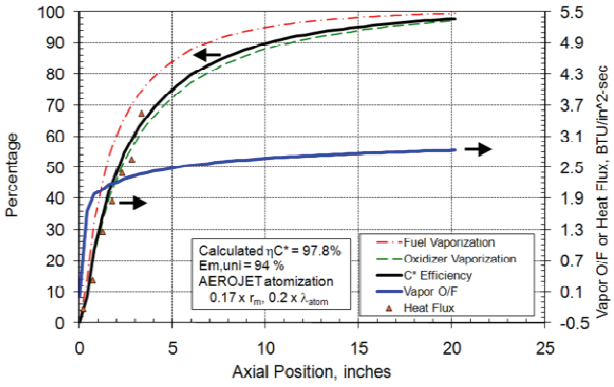


Figure 18. ROCCID analysis of 28-element swirl coax injector with $LO_2$/$LCH_4$ propellants.

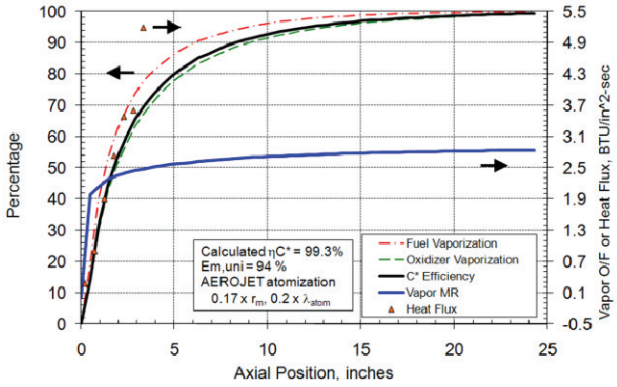


Figure 19. ROCCID analysis of 28-element swirl coax injector with $LO_2$/$LCH_4$ propellants.

Tests with a 40-element injector with swirl coaxial elements and liquid/liquid propellants where the fuel injector flow paths were redesigned showed increased performance (and apparent reduced chug oscillation amplitudes, although high-frequency pressures were not measured in this phase of the test program).[18] Modeling of these cases is slightly complicated by the diversion of some fuel from the injector element fuel flow to fuel film coolant (FFC) at the chamber wall. Consequently, in the ROCCID input file the injector pattern was split into a core zone of the inner rows and a barrier zone of the outer row into which the FFC was mixed. To provide reasonable performance calculations, ROCCID needs to mix the FFC into a barrier zone rather than leave it unmixed in an outside streamtube.

The effect on performance by altering the fuel injector coaxial annulus (or "gap") width can be examined with test data from the 40-element swirl coax element injector.[18] $\eta_{c*}$ improved from ~90-91% to ~95-96% with a reduction in fuel gap width.[18] Modeling with ROCCID for this geometrical variation was attempted but the

liquid/liquid swirl coaxial element atomization model failed to produce rational values of either fuel or oxidizer droplet sizes for the larger fuel gap widths, and reasonable values for the smaller fuel gap widths. User-defined droplet sizes were used to run the model, but little mechanistic understanding could otherwise be derived about the droplet size. The observed improvement in $\eta_{c*}$ from reducing the fuel gap widths can come from several sources – including improvement in vaporization efficiency due to better fuel atomization, improvement in vaporization efficiency due to better oxidizer atomization, and improvement in mixing efficiency due to better unielement mixing. While all possibly contribute to the performance improvement, the most likely is improvement in vaporization efficiency due to improved fuel and oxidizer atomization. An example of a ROCCID output from a test with a larger fuel gap width, and which includes heat flux data from a calorimeter chamber, is shown in Fig. 20. This calculation uses very high mixing levels as suggested from Ref. [31], but relatively large mass median droplet sizes. It is not obvious whether that is a good assumption. However, comparison of the axial $\eta_{c*}$ profile to the heat flux data suggests the selected model parameters are reasonable.

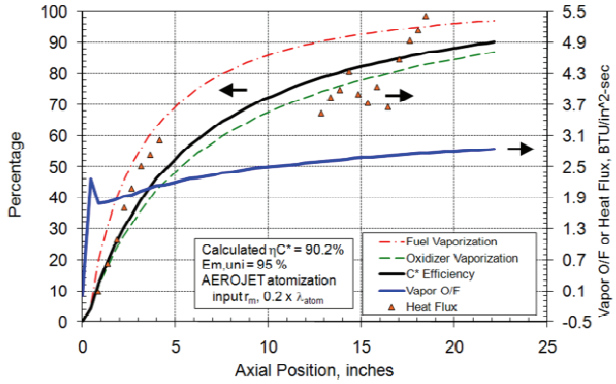


Figure 20. ROCCID analysis of larger fuel gap width 40-element swirl coax injector with $LO_2/LCH_4$ propellants.

A calculation of a test of a 40-element liquid/liquid swirl coaxial element injector with a smaller gap width in an $L'$=21" chamber is shown in Fig. 21. The predicted value of uni-element $E_m$ ~ 95% from Ref. [31] is used, along with considerable reductions in atomization length (factor of 0.2) and droplet size from the AEROJET models (factor of 0.155). A calculation with the longer combustion chamber ($L'$=25") is shown in Fig, 22. Similar to Figs. 18 and 19, $\eta_{c*}$ continues to improve with the increase in chamber length, suggesting the 40-element injector with the small fuel gap width is still vaporization limited. For these 40-element injectors, another possible performance improvement with these injector tests may be increased entrainment of the FFC into the core (i.e., improvement of inter-streamtube mixing). However, such entrainment is typically slow, and very unlikely to change sufficiently between 21" and 25" downstream of the injector face to increase $\eta_{c*}$ by the margin observed.

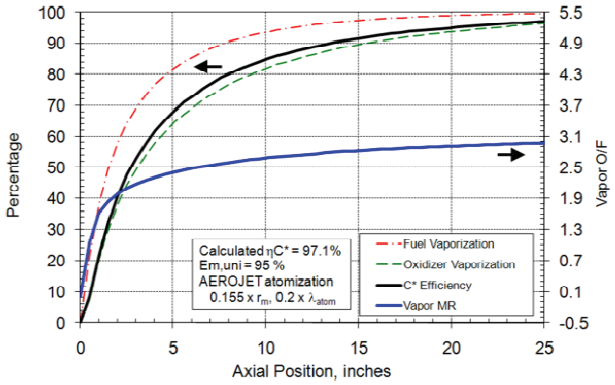


Figure 21. ROCCID analysis of 40-element swirl coax injector with smaller fuel gap width and $LO_2/LCH_4$ propellants. $L'$~21".

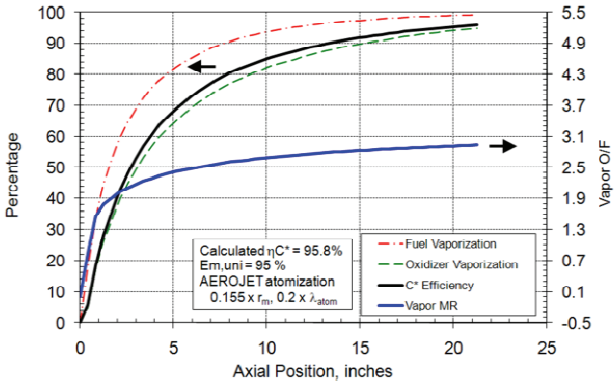


Figure 22. ROCCID analysis of 40-element swirl coax injector with smaller fuel gap width and $LO_2/LCH_4$ propellants. $L'$~25".

## B. Combustion Stability

### 1. *Low Frequency*

Nearly every test with a NASA MSFC in-house 28-element swirl coax element injector using $LO_2/LCH_4$ propellants experienced some level of low-frequency combustion instability, or "chug."[15,17] However, while the chug frequency was dominant in these tests, the waveforms of the chug oscillations often included significant high-frequency content, especially near the maximum pressure of the chug oscillation cycle. Typical waveforms from a lower $P_c$ test are shown in Fig. 23. Usually, a chug waveform is reasonably sinusoidal and not nearly so contaminated with high frequency signals. Counting higher frequency waves in Fig. 23b suggests the higher frequency is about 4000 Hz. A frequency spectrum of this signal is shown in Fig. 24, where 4000 Hz is also identified by the acoustic-like rounded signature. The spectrogram is calculated from 32768 samples over the time window as shown, with no filtering applied.

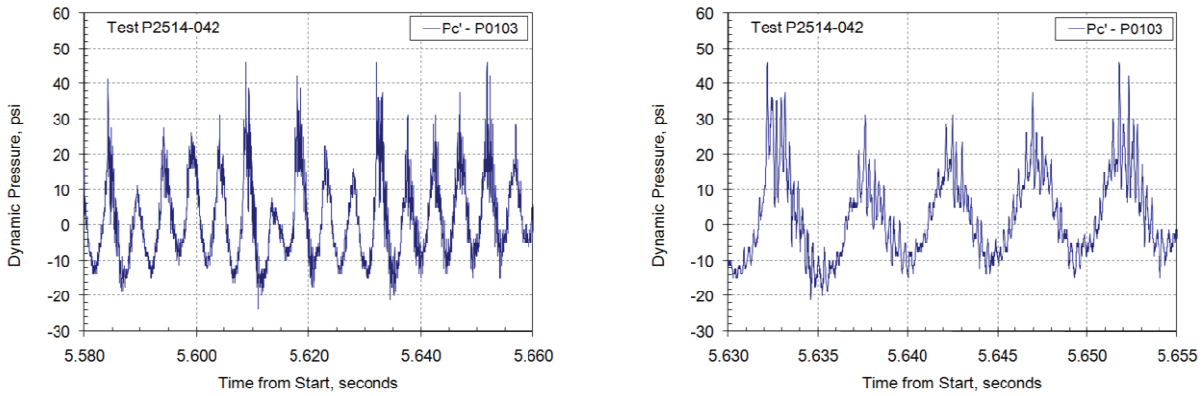


(a) View showing low-frequency content (b) Close-up showing high-frequency content

Figure 23. Chug waveform during Test P2514-042 with 28-element injector.

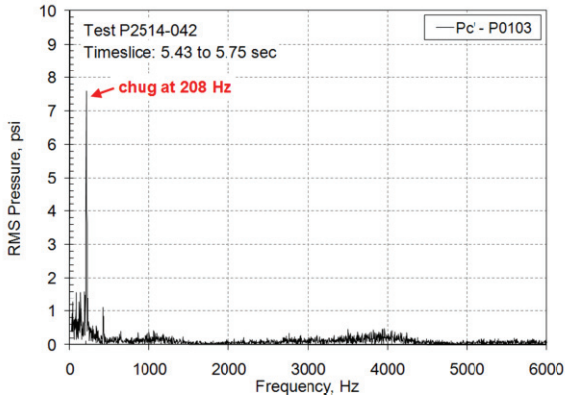


Figure 24. Spectrogram showing chug during Test P2514-042 with 28-element injector.

Throttling up (increasing the $P_c$) and lowering the *MR* significantly reduced the chug amplitude. High-frequency content was still present, but the frequency characteristics at this higher $P_c$ were different than from tests at the lower $P_c$, as will be described in a later section. In a combustion chamber approximately with half the length, significantly increased chug amplitude was observed, while in a longer combustion chamber chug amplitude was reduced. Both changes were predictable from changes in $L^*$.

Similar chug characteristics except with higher overall amplitudes were encountered during tests with an initial 40-element swirl coax element injector.[17] Following this test, several broken oxidizer swirl metering orifices were found loose in the oxidizer manifold, and several other metering orifices were found with bulged or shattered slots.[17]

An injector element redesign which reduced the oxidizer slot metering area and revised the fuel sleeve geometry also experienced chug, and, later in the same test, spontaneous 1T combustion instability.[17] The higher oxidizer pressure drop reduced the chug amplitude, while the character of the high-frequency content in the spectrum appeared unchanged. Following this test, several broken oxidizer swirl metering orifices were again found loose in the oxidizer manifold, with another metering orifice also found with bulged slots.[17]

Initial tests with a further redesigned 40-element injector pattern using the reduced oxidizer metering configuration that had previously been unstable at the 1T mode, plus a change of the fuel sleeve design, showed similar or worse chug characteristics during initial tests.[18] Unfortunately, high-frequency pressure was not measured during these initial tests, but only during a limited test series with a calorimeter chamber. Later variations of the fuel annulus design with reduction of the fuel gap widths in later tests appeared to improve chug stability characteristics. However, no high-frequency pressure was measured in these tests, and static pressure measurements recorded on high-speed data systems appeared unreliable as several tests had inconsistent results – i.e., considerable chug amplitude on one test and then little on a later test with similar test conditions. These data are still under review.

Chug test data were compiled and compared to attempt to determine the experimental neutral chug stability curve, the measured boundary between stable and unstable operation. Compiled data for the 28-element injector are shown in Fig. 25. Data are either marginal (M) or unstable (U/S) except for one test, and would be at or below the neutral stability curve. Unfortunately, a second test series using the same injector also had a 20% reduction in fuel injector admittance (flowrate/square root of pressure drop), which compromises the analyses. The oxidizer injector admittance was similar between the test programs, so the chamber pressure during chug was not a suspected error. No explanation for the change in the fuel injector admittance has been found.[17]

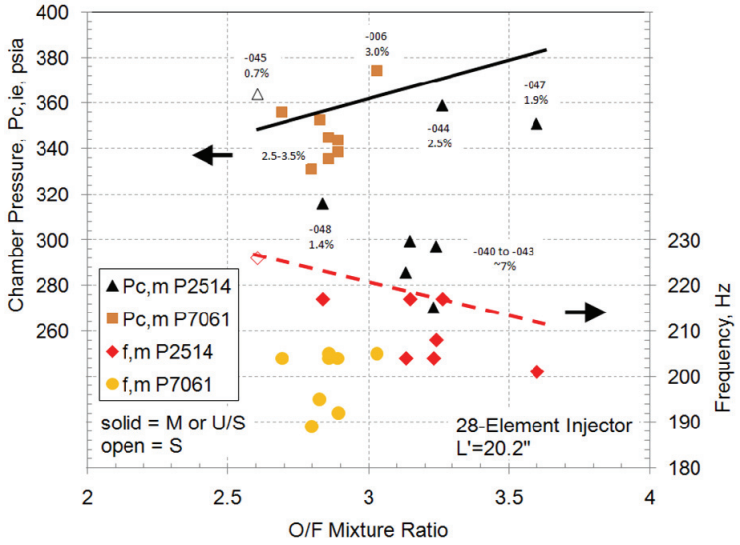


Figure 25. Compiled chug data and model prediction for the 28-element injector. Data = points, model prediction = lines.

Modeling of the chug was conducted with the techniques described by Wenzel & Szuch.[36] This analysis procedure defines the neutral chug stability curve from the solution of a linearized characteristic equation describing instability in a lumped-parameter impedance combustion chamber. Each propellant has its own specific time lag, a delay time which is a function of injection thermodynamics, chamber pressure, and mass flow rates. A mixing time lag common to both propellants is also included. Errors in the characteristic equation shown as equation (31) in Ref. [36] were corrected in the current analyses. The model was applied to match the characteristics of the neutral stability curve defined from evaluation of the data in Fig. 25, including the observed frequencies of oscillation at the respective chamber pressures. The results of the modeling are shown in Fig. 25. A solid black line represents the neutral stability curve defining the insipient chamber pressure at chug, and a red line represents the frequencies at the neutral stability curve.

To force the model to generate the predictions shown in Fig. 25, only a portion of the total measured fuel injector pressure drop was allowed, which means some of the pressure drop was not participating in resisting chug. The fuel annulus sleeve designs for the data in Fig. 25 were unusual for coaxial injector design in that most of the fuel

injector pressure drop was located in the fuel sleeve holes rather than in the annulus or exit dynamic head.[15,17] Unlike for liquid oxidizer/gaseous fuel injectors, increased fuel pressure drop for liquid oxidizer/liquid fuel injectors is stabilizing. However, to stabilize the system shown in Fig. 25 for expected conditions (about $P_c$ = 250 psia) will require increasing $\Delta P/P_c$ for both injector circuits.

A revised fuel annulus sleeve design that applied the majority of fuel injector pressure drop to the annulus or exit dynamic head rather than the fuel sleeve holes was used in the later tests with the 40-element injector, along with a higher-pressure drop oxidizer circuit.[18] Unfortunately, for these tests high-frequency pressure was not measured, so reliable dynamic data were not available. Preliminary evaluations with static pressure recorded at high sample rate suggest that increased $LCH_4$ injector pressure drops at the injector element exit and increased $LO_2$ injector pressure drop improved chug stability margin for these tests. Final analysis results of these data are not yet available.

2. *High Frequency*

No test with the 28-element swirl coax element injector exhibited sustained combustion instability at a longitudinal or transverse acoustic mode of the combustion chamber. However, high-frequency content, especially between 2500-4000 Hz, was always present in the chamber pressure, and contaminated the low frequency signal during chug oscillations, as shown for example in Fig. 23b. If the chug frequency would be removed by high-pass filtering, the remaining higher frequency waveforms in Fig. 23b would resemble resurge instability. Whether what is seen in Fig. 23b is resurge, especially when compared to other 28-element injector tests, is still under investigation. More detailed stability data and analyses from these tests are available in Ref. [37].

Two different forms of high-frequency content were observed during tests with the 28-element injector. The first, at lower $P_c$s (270-300 psia), had a single rounded response with a frequency at the peak amplitude around 4000 Hz, and other minor content except for 1100 Hz. The second, at higher $P_c$s (315-375 psia), had several distinct peaks centered around two frequency ranges – one at 2400 Hz to 3600 Hz, the other at 4800 Hz to 5300 Hz. Planar frequency intensity plots for representative tests of each form are shown in Figs. 26 and 27, and spectrograms for these tests are shown in Figs. 28 and 29.

For the test shown in Fig. 28, an equilibrium 1T mode acoustic frequency is calculated to be about 5015 Hz, and a first longitudinal (1L) mode acoustic frequency is calculated to be about 1240 Hz. Figure 28 shows two obvious high-frequency signatures at about 1100 Hz and 4000 Hz, and possibly several others including 2800 Hz, 3500 Hz, and 5500 Hz. Longitudinal and transverse acoustic modes that are not unstable are often observed at lower frequencies than calculated by the equilibrium combustion sound speed, so the observed frequency of 4000 Hz (or an effective sound speed ~80% of equilibrium) would not be unrepresentative for a 1T acoustic mode. Likewise, at an effective sound speed ~90% of equilibrium, the 1100 Hz signal might be the 1L mode. Unfortunately, there was insufficient high-frequency pressure instrumentation in the combustion chamber to verify that what was observed at 4000 Hz was the 1T mode.

The RMS pressure amplitudes for the signal at 4000 Hz shown in Fig. 28 represent fairly small amplitude waves, typical for an unexcited acoustic mode. However, the amplitudes of the 4000 Hz oscillation at the maximum pressure of the chug wave as shown in Fig. 23(b) are much larger, ~ 20 psi peak-to-peak (~7 psi RMS), or almost as large as the amplitude of the chug oscillation itself. The spectrograms in Figs. 24 or 28 thus are not good portrayals of the real character of the high-frequency oscillations shown in Fig. 23.

The spectrogram for the higher $P_c$ test shown in Fig. 29 has a different character than for the low $P_c$ test shown in Fig. 28. Equilibrium acoustic frequencies were nearly identical with the lower $P_c$ tests, despite considerable differences in $P_c$ and sometimes *MR*. Figure 29 identifies four or five peaks of acoustic-like behavior at the higher $P_c$ – 5100-5200 Hz, 3400-3500 Hz, 2500-2800 Hz, and 1000 Hz. The chug is still identifiable between 165 and 230 Hz. Closer examination of raw waveforms of several of these higher-pressure 28-element injector tests reveals that while there was no sustained high-frequency instability, several tests displayed bursts of short-duration spontaneous instability. Results of an instructive test, at high $P_c$ and low *MR* where peak-to-peak chug amplitudes had been reduced to less than 1% of mean $P_c$, is shown in Fig. 30. In this test, numerous periods of extended spontaneous high-frequency instability occurred, lasting 15 to 40 msec, several indicated by the arrows in Fig. 30. A close-up of a waveform during one of those bursts is shown in Fig. 31, clearly indicating multiple frequencies. Figure 32 compares spectrograms of a narrow time slice of one of the bursts to a longer average time. The spectrogram over the longer time slice is similar to Fig. 29, showing peaks of high-frequency behavior at 5100 Hz, 3400 Hz, 2500 Hz, and 990 Hz. However, the spectrogram over the narrow time slice in Fig. 32 shows that two of those signals – at 2540 and 5080 Hz – have been excited, along with another signal at 7620 Hz. The 5080 Hz signal in Fig. 32 could be the 1T mode, nearly exactly at the equilibrium value, which may have been excited by the signal at 2540 Hz.

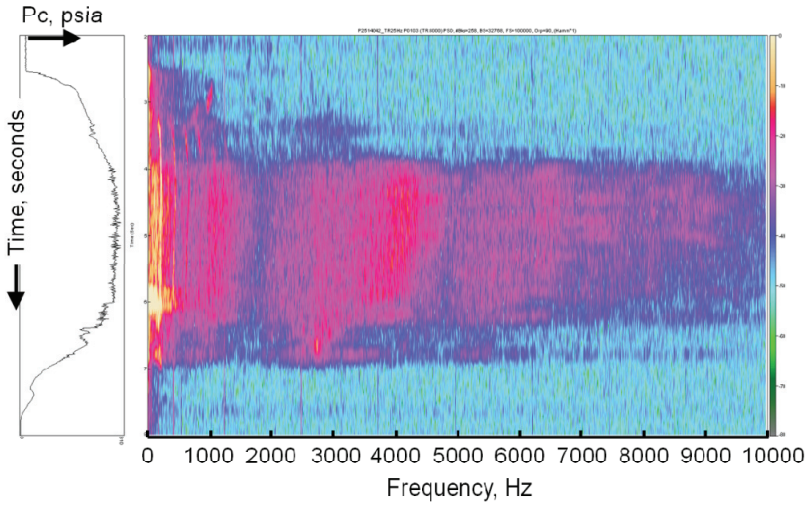


Figure 26. Planar spectrogram of high frequency pressure from low-$P_c$ test with 28-element injector. Test duration increases from top to bottom. Color scale at right is decreasing RMS pressure from top to bottom. The plot at left shows static chamber pressure.

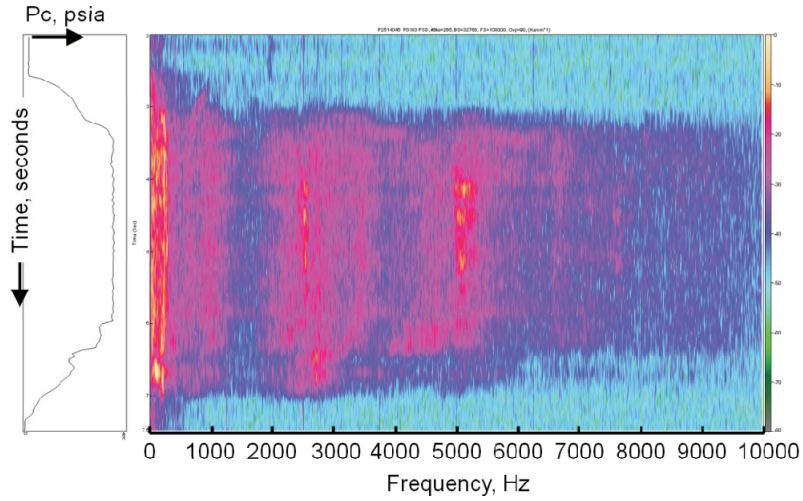


Figure 27. Planar spectrogram of high frequency pressure from high-$P_c$ test with 28-element injector. Test duration increases from top to bottom. Color scale at right is decreasing RMS pressure from top to bottom. The plot at left shows static chamber pressure.

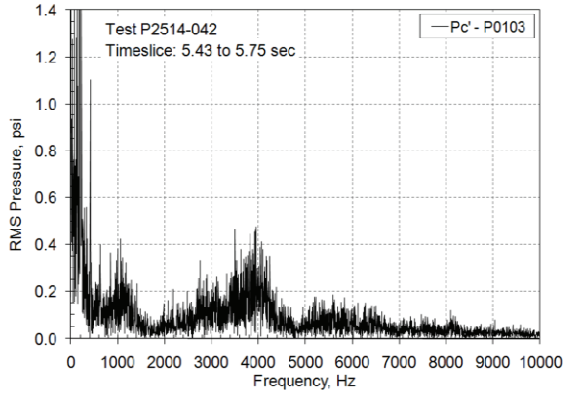


Figure 28. Spectrogram of low $P_c$ test with 28-element injector.

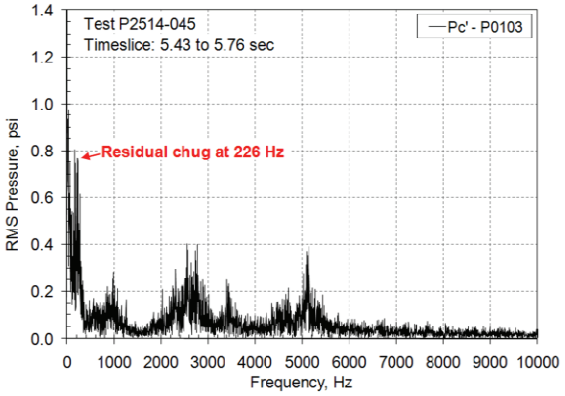


Figure 29. Spectrogram of high $P_c$ test with 28-element injector.

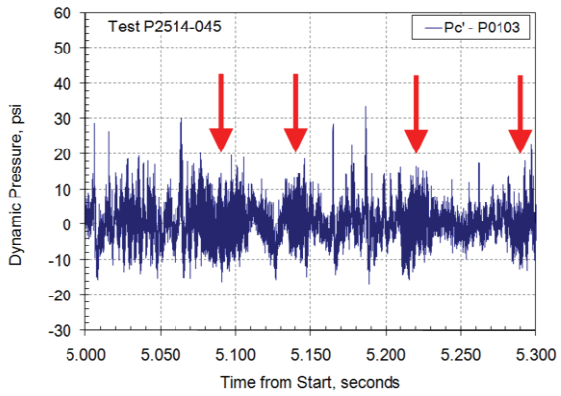


Figure 30. Pressure time trace during Test P2514-045 with 28-element injector.

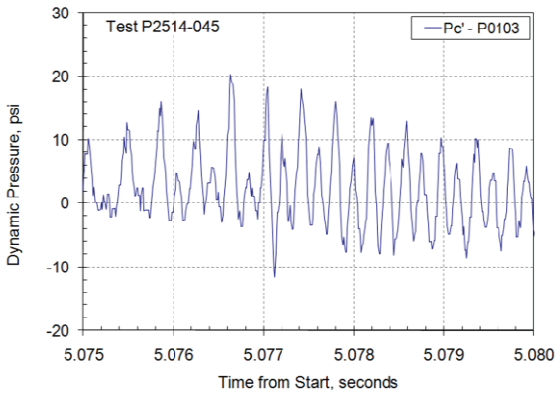


Figure 31. Waveform of high-frequency activity during Test P2514-045.

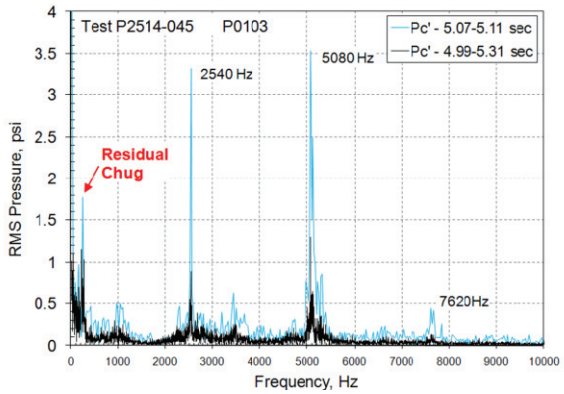


Figure 32. Spectrograms from Test P2514-045 during high-frequency activity.

Since the bursts of high-frequency activity shown in Figs. 30 to 32 were not sustained, and were not the result of dynamic stability rating perturbations, they present some challenges for categorization when consulting combustion stability guidelines such as Ref. [38]. The oscillation at 5.08 seconds in Fig. 30 is obviously discrete and well above the amplitudes of the noise floor or the averages of the transverse acoustic modes. The peak-to-peak amplitude of the oscillation at 5.08 seconds is 3% to 5% of the mean chamber pressure, relatively small but not typically acceptable for transverse mode stability for flight vehicles. Had the high-frequency event at 5.08 seconds been the result of a dynamic stability rating perturbation, the damp time of 37 msec would have exceeded the allowable damp time according to Ref. [38], calculated to be about 18 msec for the frequency at 5080 Hz if that is the 1T mode.

Understanding the high-frequency combustion stability characteristics of these tests requires identifying the sources of the signals shown on Figs. 26-32. Because of insufficient high-frequency pressure instrumentation during these tests, it is not readily apparent what these signals represent. Sources of such signals can include sensor tube resonances, dynamics of injector element features such as the oxidizer tube or the fuel annulus, or dynamics of combustion processes such as atomization, vaporization, mixing, and reaction. Two can be quickly excluded: 1) the sensor tube resonance of the high-frequency pressure transducer, according to sensor port configurations, is about 50 kHz, and 2) the quarter-wave resonance of the fuel annulus of the injector element is about 11 kHz.

Axial (or "organ pipe") resonances of the flow in the oxidizer tube of a shear coaxial injector element have been recognized for some time as sources of combustion instability in coaxial element injectors,[7,32,39,40] and calculating such resonances in a shear coax element oxidizer tube is fairly straightforward. However, the dynamics of a hollow-core swirl flow in a tube are more complicated.[41] As first order estimates, simple calculations of quarter-wave (closed/open acoustic) resonances are usually close to the relevant frequencies, since the upstream end of the injector element is usually metered and approximates a closed acoustic boundary. For the 28-element injector swirl coax element, a quarter-wave resonance of the annular oxidizer film attached to the tube wall could be about 1500 Hz, while a quarter-wave resonance of the gaseous fluid in the center depends on the composition of the gas and can range from 400 Hz with cold gaseous oxygen to 2600 Hz with equilibrium combustion products. These calculations suggest the 2500-2800 Hz signals in Figs. 26-32 may be resonances of the gaseous core in the oxidizer tube.

Another source for high-frequency combustion instability has been suggested by Hewitt.[34,35] The Hewitt Stability Correlation is based on a parameter *d/V* – injection orifice dimension *d* divided by injection velocity *V* of the least volatile propellant – that describes observed combustion instability of like-on-like doublets with storable propellants.[34] The correlation has been extended to other propellant combinations and element types[42,43] including swirl coaxial elements with liquid oxygen and dense gaseous hydrogen.[44] For the latter, with the assumption that this element responds like an unlike doublet (due to direct impingement of unlike propellant streams), the injection orifice dimension *d* has been expressed as the film thickness of the hollow-cone swirl flow as calculated by a method such as Doumas and Laster.[45]

While in most applications the fuel is the least volatile propellant, for $LO_2/LCH_4$ propellants the $LO_2$ is the lesser volatile, although the volatilities are much more similar compared to other propellant combinations such as oxygen/hydrogen or oxygen/kerosene. Consequently, for this paper both propellants will be analyzed. For the $LCH_4$, the injection orifice dimension *d* is suggested to be either the fuel annulus "gap width" or the hydraulic diameter of the fuel annulus, which is the twice the gap width.

The Hewitt Stability Correlation has been presented two ways, with *d/V* as a function of chamber diameter in which instability was observed, or with *d/V* as a function of the maximum sustainable frequency of instability which can be supported by that *d/V*, which is a function of element type but not propellant combination.[34,35] Using the latter method for both $LO_2$ swirl film and $LCH_4$ annular flows predicts a range of maximum sustainable frequencies of instability squarely in the range of frequencies observed in the test data. Maximum sustainable frequencies of instability from *d/V* range from 2700-3700 Hz for the $LO_2$ swirl film (assuming film thickness for *d*), and from 2000-3000 Hz for the $LCH_4$ annular flow (assuming gap width for *d*). Similar frequencies from periodic spray oscillations have been measured in cold flow tests of hollow-cone swirl flows.[46]

However, if the combustion system is responding to *d/V*-generated frequencies, the frequencies should show a functional relationship to *V*. Measured frequencies of signals obviously above the noise floor in five frequency ranges – around 1000 Hz, 2500 Hz, 2800 Hz, 3500 Hz, and 5000-5500 Hz – were essentially constant versus calculated oxidizer and fuel injection velocities. These data suggest that these particular frequencies are likely to be resonances of injection element features or acoustic modes of the combustion chamber. Comparing to predictions using equilibrium combustion product sound speed, the signals at 1000 Hz are likely the 1L mode and the signals at 5000-5500 Hz are likely the 1T mode. The 2500 Hz, 2800 Hz, and 3500 Hz are thus likely to be resonances of the oxidizer post. Certainly a calculation of a 2500 Hz resonance frequency of the swirl coaxial element from a gaseous core with combustion product sound speed is encouraging.

While these discussions provide preliminary rationale for most of the observed frequencies, there is still no clear rationale for one of the major differences between Fig. 26 and Fig. 27, which was the disappearance of the 4000-Hz signal at lower chamber pressures when throttling up to higher chamber pressures. A rationale for that may be provided by examination of 40-element swirl coax element injector test data.

Three tests with two different configurations of 40-element injectors had high-frequency instabilities near 4500 Hz apparently at the first tangential (1T) acoustic mode of the combustion chamber. With only one high-frequency pressure sensor in the combustion chamber, positive identification of the unstable mode was not possible. However, the measured frequency was found to be about 90% of that calculated with equilibrium sound speed for the 1T mode in all three cases. Also, in one test which occurred in a calorimeter chamber, there was a dramatic increase (about a factor of ten near the injector) in measured circumferential heat flux in the combustion chamber. Had the high-frequency oscillation been only due to excitation of element resonances, it is unlikely the heat flux would have increased so dramatically. These factors suggest that the 4500-Hz oscillation was an unstable 1T mode. Unfortunately, most of the tests with variations of 40-element injector features did not contain high frequency pressure sensor measurements, either in the chamber or the injector manifolds, or any accelerometer data, so it was not possible to characterize the high-frequency stability of these tests or their hardware changes.

The first two apparent 1T instabilities with the 40-element injector occurred with the first two tests of a new oxidizer element with a smaller metering orifice than used in initial testing. A planar frequency intensity plot of one test is shown in Fig. 33. The onset of instability is clearly seen at 4550 Hz, along with the appearance of a harmonic at 9100 Hz; higher frequency harmonics can be seen in the spectrum up to a test facility low-pass filter cut-off at 20 kHz. Waveforms immediately before and during the transition to the instability are shown in Fig. 34, illustrating the transition from chug to high-frequency instability. Figure 34(a) shows the spontaneous excitation of a 3910 Hz oscillation from one chug cycle, lasting about 8 msec. Note in Fig. 34(b) that the instability was initiated at the maximum pressure of the chug oscillation cycle, where similar high-frequency dynamics have been observed from nearly all tests. This result resembles the unstable outcome from a perturbation of a dynamic stability rating test. A waveform of the high-frequency instability is shown in Fig. 35. Spectrograms immediately before and after the instability are shown in Figs. 36 and 37.

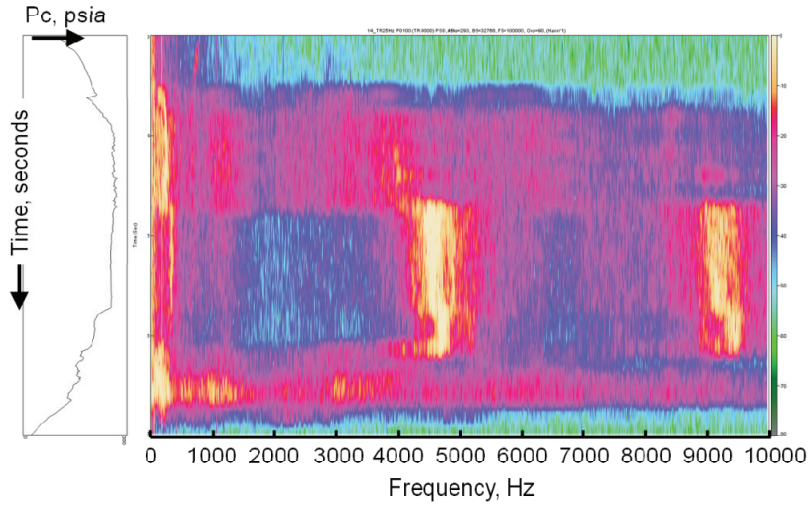


Figure 33. Planar spectrogram from Test P7061-014 showing high-frequency instability. Test duration increases from top to bottom. Color scale at right is decreasing RMS pressure from top to bottom. The plot at left shows static chamber pressure.

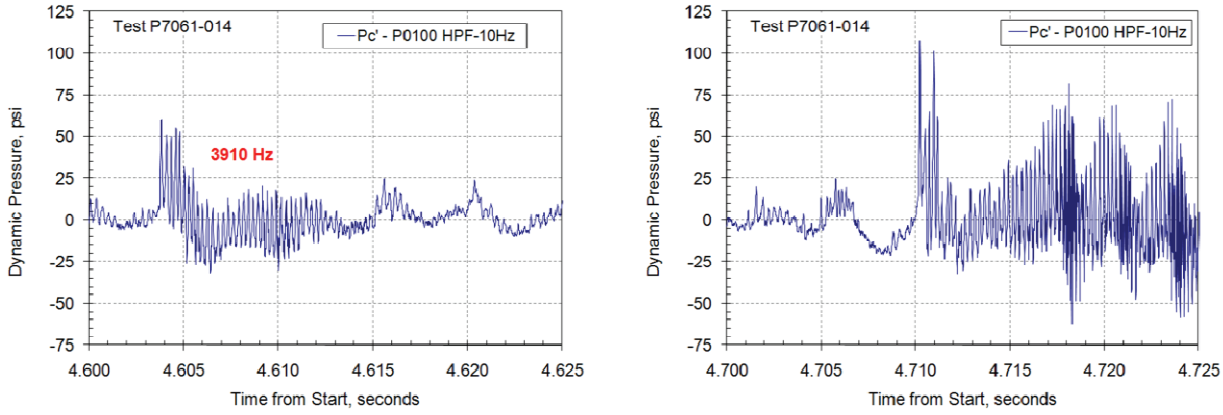


(a) Before onset of high-frequency instability (b) Transition to high-frequency instability

Figure 34. Waveforms from Test P7061-014 of chug and transition to high-frequency instability.

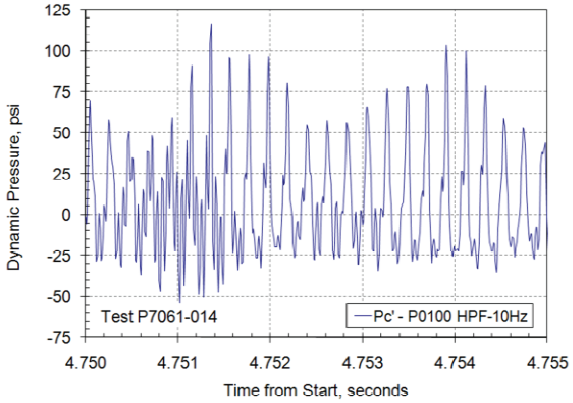


Figure 35. Waveforms from Test P7061-014 of high-frequency instability

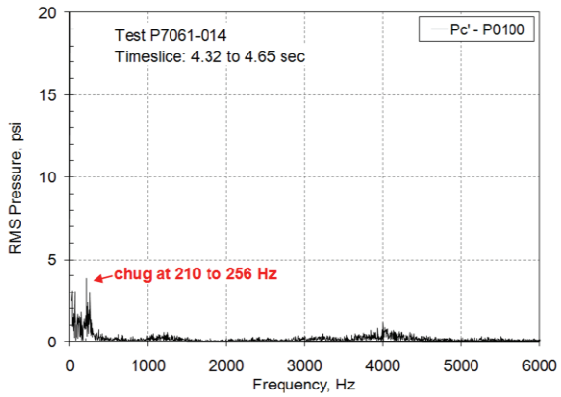


Figure 36. Spectrogram showing low-level chug prior to high-frequency instability during Test P7061-014 with 40-element injector.

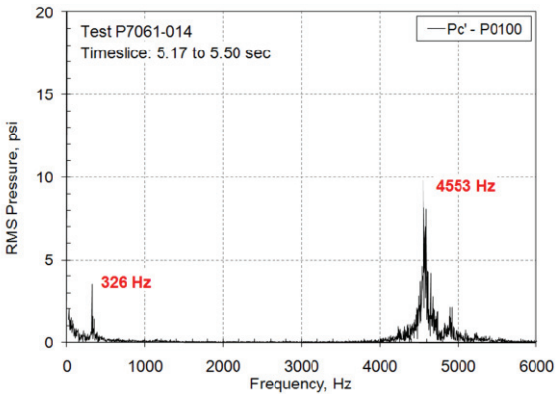


Figure 37. Spectrogram showing high-frequency instability during Test P7061-014 with 40-element injector.

For the high-frequency instability shown in Figs. 33, 35, and 37, peak-to-peak amplitude is observed to be about 10% of the mean chamber pressure, which is not especially large for transverse mode instability, although only one transducer was available for this measurement and the maximum amplitude may not have been measured. Perhaps more concrete proof this actually was transverse mode instability is provided by a test of a similar injector but in a calorimeter instead of ablative chamber.

High-frequency instability occurred about 1.6 seconds after initiation of $LCH_4$ on this test. Figure 38 shows the transition from chug to high-frequency instability. The dynamic nature of this transition, starting from the peak of the chug oscillation cycle, closely resembles Fig. 34(b). A spectrogram of this instability is shown in Fig. 39. Unfortunately, this transducer failed shortly after the time shown. The heat flux in the combustion chamber in this test, measured with water-cooled calorimeter spools, increased dramatically within 1.5 seconds after the initiation of the instability, as shown in Figs. 40 and 41. The test was terminated just after the time of the latest heat flux average shown on Fig. 40 due to high calorimeter outlet water temperature.

An 8- to 12-times increase in heat flux at the injector face as indicated by Fig. 40, along with nearly a doubling of heat flux in the barrel and at the throat, is certainly the result of high-frequency combustion instability at a transverse acoustic mode of the combustion chamber. The only possible mode for this frequency is the 1T, as predicted at a frequency about 90% of that calculated with equilibrium sound speed. Instabilities due to coupling to injector features such as oxidizer post modes have not been observed to develop such thermal distress.

This instability has different characteristics than the short duration spontaneous instability shown in Fig. 32 for the 28-element injector – no apparent source frequency such as the 2540 Hz signal is apparent in Figs. 37 or 39. For this and the other two high-frequency instabilities, the Hewitt Stability Correlation provides some guidance. Hewitt *d/V* are plotted versus chamber diameter in Figs. 42 and 43 for oxidizer and fuel, respectively, where *d* for oxidizer is film thickness and *d* for fuel is gap width.

Several key aspects can be diagnosed from Figs. 42 and 43. Foremost, comparison of the oxidizer *d/V* using oxidizer swirl flow film thickness as *d* predicts three 40-element injector tests conducted with smaller oxidizer metering features that went unstable to be unstable at the 1T mode of the undamped 5.66" diameter combustion chamber. Tests with 40-element injectors with larger oxidizer metering features, which were chugging and had rich high-frequency content but did not have sustained high-frequency instability, are located in a more stable zone between the ½-1T line and 1T line, as shown in Fig. 42. Injectors located between the ½-1T line and the 1T line most likely will require combustion chamber damping devices for stabilization.[35] No damping devices were included in any of the 5.66" diameter chamber tests.

Second, oxidizer *d/V* for the 28-element injector tests, also located between the ½-1T and 1T lines, are likely to be stable or marginal in 1T in undamped combustion chambers, and have increased levels of high-frequency content in the dynamic data, which is also exactly what was observed. Also, while the maximum sustainable frequencies from oxidizer *d/V* shown in Fig. 42 for the 28-element injector do not support instability, the proximity to the 1T line suggests some influence of the 1T mode. This is the proposed reason why 4000-Hz signals in lower chamber pressure tests (at lower oxidizer velocities) become 4500-5000-Hz signals at higher chamber pressure tests (at higher oxidizer velocities).

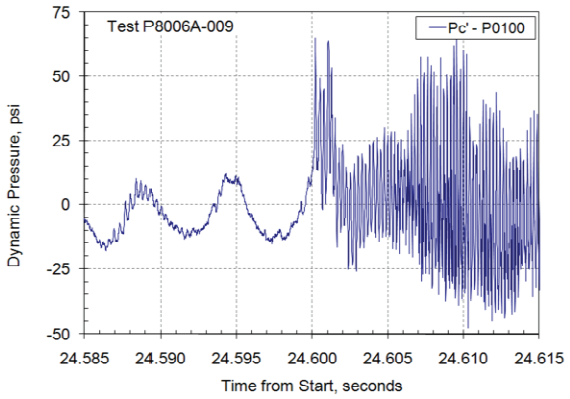


Figure 38. Transition from chug to high-frequency instability during Test P8006A-009.

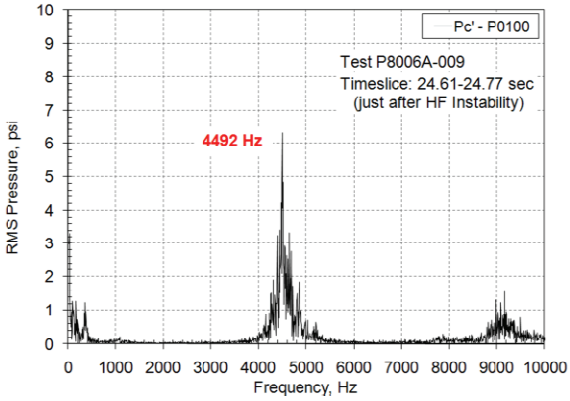


Figure 39. Spectrogram of high-frequency instability during Test P8006A-009.

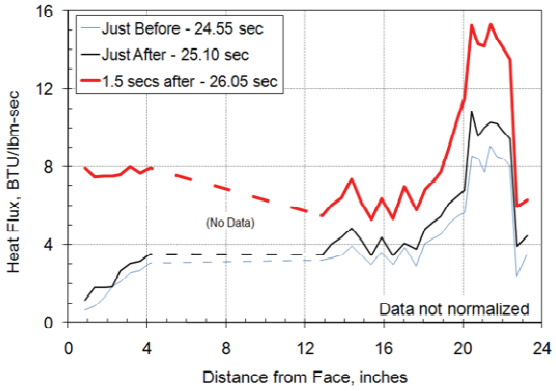


Figure 40. Increase in measured combustion chamber axial heat flux due to high-frequency instability in Test P8006A-009.

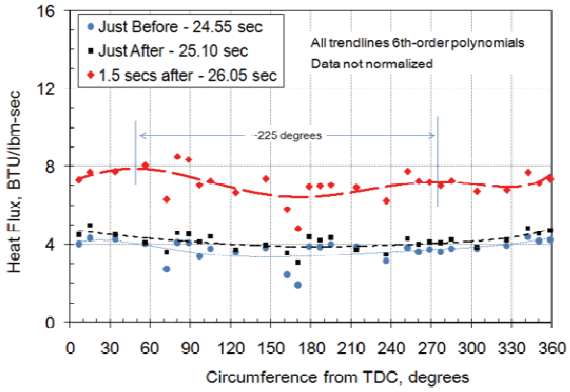


Figure 41. Increase in measured combustion chamber circumferential heat flux due to high-frequency instability in Test P8006A-009.

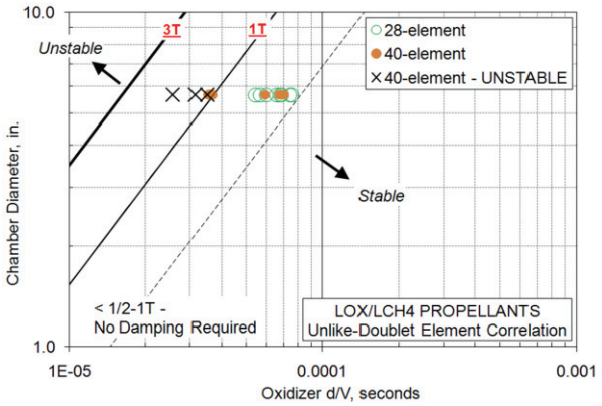


Figure 42. Hewitt Stability Correlation for unlike doublets, with oxidizer *d/V* calculated for the swirl coax with *d* as oxidizer film thickness.

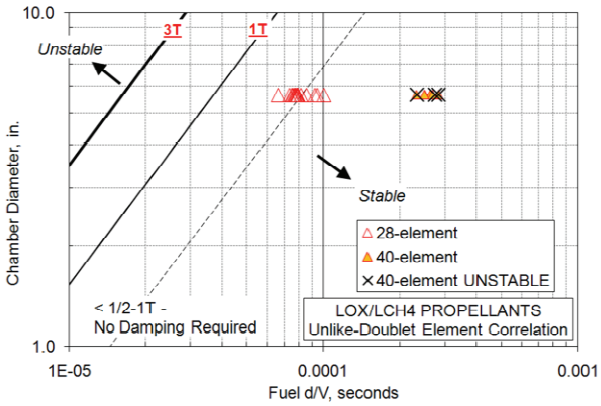


Figure 43. Hewitt Stability Correlation for unlike doublets, with fuel *d/V* calculated for the swirl coax with *d* as fuel gap width.

Finally, comparison of the fuel *d/V* using fuel gap width as *d* as shown in Fig. 44 predicts the 40-element injector tests to be stable, contrary to the evidence. Thus, from a *d/V* perspective, the $LCH_4$ circuit is not the driving source for instability in these tests. For the 28-element injector, Fig. 43 shows the fuel system is less stable, so in tests of that injector the fuel may be generating high-frequency content.

## IV. Summary and Conclusions

As part of an effort funded by the Propulsion and Cryogenic Advanced Development (PCAD) project, under the Exploration Technology Development Program, the NASA Marshall Space Flight Center has been evaluating combustion performance and stability modeling capability for oxygen and methane propellants. The purpose of conducting these analyses was to evaluate the capability of currently available methods to predict combustion, performance and stability characteristics for future development of liquid rocket engine combustion devices with methane propellant.

Combustion performance analyses have been conducted on several rocket engine thrust chamber configurations using liquid oxygen and gaseous and liquid methane propellants where characteristic velocity performance could be evaluated. For several of these cases, axial heat flux profiles were available as well, which provided an additional anchoring technique to the combustion analyses. The results of performance analyses of the selected $LO_2/CH_4$ test cases with the ROCCID and CICM codes provided mixed results. The ROCCID code provided acceptable predictions for single-element shear coaxial element injectors with liquid oxygen and gaseous methane propellants at higher chamber pressures (greater than about 600 psia), using the Burick correlation for $E_m$ and a 30% increase in the DROPMIX droplet size. However, predictions for throttled conditions (low chamber pressures ~300 psia), given anchoring at higher chamber pressures, were unacceptable. Operating conditions at the low chamber pressures were within the range of a mixing correlation for shear coaxial elements, but use of the mixing correlation significantly over-predicted performance. Additional mixing, atomization and hot-fire test data are necessary to examine the discrepancies at these conditions.

The CICM code also provided reasonable results for single-element shear coaxial element injectors with liquid oxygen and gaseous methane propellants at higher chamber pressures when new atomization anchoring parameters were used. The manual-suggested inputs for cup and chamber atomization parameters, which were developed from oxygen and hydrogen propellant engines, were not valid with oxygen and methane propellants. Development of new atomization parameters with recommended methods was not successful since cup pressure drops in the $LO_2/gCH_4$ test cases were negligible. Consequently, parametric analyses were conducted to determine a set of parameters that could best fit the test data. Two of the four atomization parameters were found to be influential. Calculations with these parameters provided reasonable comparisons to both performance and axial heat flux profile data, but like with the ROCCID cases, only at higher chamber pressures (greater than about 600 psia). At the low chamber pressures for throttled conditions (300 psia) where ROCCID over-predicted measured performance, analyses with CICM greatly under-predicted the measured performance.

With swirl coaxial elements with liquid oxygen and gaseous methane propellants, significant alterations of atomization parameters calculated within ROCCID and $E_m$ from available correlations were required to match measured performance and energy release rates suggested by axial heat flux profile measurements. Significant improvements in mixing and atomization predictions are required for swirl coaxial element injectors.

For cases with liquid methane with multi-element LOL impinging element injectors, ROCCID provided acceptable predictions using the Nurick correlation for $E_m$ and the DROPMIX atomization parameters as calculated in ROCCID. With swirl coaxial elements, significant changes were again required for the calculations of atomization parameters within ROCCID. The atomization calculation for both the swirled liquid oxidizer flow and the annular liquid fuel flow required extensive modifications to fit to the measured data, and failed outright for elements with large fuel annulus widths. However, use of quasi-anchored parameters predicted the vaporization-limited performance that likely occurred with several of the cases. Significant effort is required to improve the capability to make such predictions.

Combustion stability characteristics of several multi-element swirl coaxial element injectors with $LO_2/gCH_4$ propellants were examined and correlated with simple models. These injectors were designed, fabricated and tested by the NASA MSFC with funding from PCAD. Low frequency combustion instability (chug) occurred with most injector patterns, with frequencies ranging from 150 to 250 Hz. While several tests with a 28-element injector had low peak-to-peak chug oscillation amplitudes (0.7%-4% of mean chamber pressure), no test appeared to be completely free of chug influence, even at chamber pressures exceeding 360 psia and mixture ratios as low as 2.6. Modeling with the methods of Wenzel and Szuch showed the influence of chamber pressure, mixture ratio and

$LCH_4$ injector pressure drop on neutral chug stability. Increasing $LCH_4$ injector pressure drop at the injector element exit was predicted to improve chug stability margin for the 28-element injector, although stabilization at desired operating conditions will require increased injector pressure drops on both circuits. Tests with a 40-element injector with low $LCH_4$ injector pressure drop at the injector element exit exhibited similar chug characteristics. A later revision of the 40-element injector with increased $LCH_4$ injector pressure drop at the injector element exit as well as increased $LO_2$ injector pressure drop appeared to improve chug stability, although reliable dynamic data were not available for these tests.[18]

All tests with the 28-element swirl coax element injector and the handful of tests with the initial 40-element swirl coax element injector patterns that included a high-frequency pressure sensor showed a rich high-frequency dynamic environment in the undamped combustion chambers. The chug oscillations for these injectors were contaminated by high-amplitude, high-frequency ringing at the maximum pressure of the chug oscillation cycles, with some bursts lasting several tens of milliseconds, suggesting such injector patterns might be unstable in dynamic stability rating tests in these undamped combustion chambers.

High-frequency chamber pressure dynamics with the 28-element injector appears to be the result of two phenomena – oscillations of the gaseous core in the oxidizer post, and high-frequency instabilities due to unsteady atomization of the conical oxidizer film. For the former, simple estimates of "organ pipe" frequencies of the gaseous core compared reasonably well to some observed oscillation frequencies. Spontaneous bursts of high-frequency activity from such an oxidizer post mode may have excited the 1T mode on several tests, exceeding allowable damp times for the 1T mode. Mechanistic models to predict the responses of such oxidizer post "organ pipe" oscillations for a hollow-core swirl coaxial element are in development. Note that while this post resonance may have been destabilizing in the current case, the use of a properly tuned gas core resonance as a stabilizing feature is also possible.[47] For the atomization-dependent phenomenon, the Hewitt Stability Correlation provided a reasonable rationale for low-amplitude excitement of near-1T mode frequencies that changed with chamber pressure (actually, oxidizer injection velocity).

High-frequency chamber pressure dynamics with the initial 40-element swirl coax element injector patterns for which a high-frequency pressure sensor was available appeared similar to the 28-element injector dynamics, except that the 40-element injector was more sensitive to the 1T mode. High-frequency combustion instability occurred in three tests apparently at the 1T mode with initial versions of the 40-element injector, evident by a frequency measured with a single high-frequency chamber pressure measurement as well as a dramatic increase in head-end chamber heat flux measured in one test with a calorimeter chamber. The occurrences of these instabilities correlated closely with predictions from the Hewitt Stability Correlation using oxidizer film thickness as a correlating parameter. These results suggest that the 40-element injector pattern (and most likely the 28-element injector pattern as well) would require combustion chamber damping devices for high-frequency stabilization.

## V. Recommendations for Future Work

It is apparent that *a priori* predictions from the non-CFD codes of combustion, performance and stability that were examined with methane (and especially liquid methane) propellant are not in a reliable state to support design of new combustion devices with this propellant. The primary errors appear to extend from failure to predict atomization characteristics. Some element types are in a better state of readiness than others, e.g., shear coaxial elements with gaseous methane and like-on-like doublet elements with liquid methane. Also, in several cases when anchored to hot-fire test data, the existing codes can predict combustion performance reasonably well, with the exception of deep throttled conditions. For high quality predictions, data for similar geometries are needed to anchor the prediction.

However, improvement of capability to calculate *a priori* combustion, performance and stability will be necessary for the cost-effective development of new combustion devices for liquid rocket engines using methane. The following list provides recommendations for the improvement of combustion performance analysis modeling techniques with $LO_2/gCH_4$ and $LO_2/LCH_4$ propellants.

1) Extend the Burick shear coaxial element Rupe mixing efficiency ($E_m$) correlation for conditions with methane fuel. Use of an element with the higher densities of methane (or any fuel denser than gaseous hydrogen) required extrapolation beyond the range of the correlation in all cases except at the very low chamber pressures, when it appeared that the mixing efficiency from Burick was significantly overpredicted. The mixing efficiencies could be derived experimentally or computationally. Calculating the mixing efficiency numerically would be acceptable, given the predictions are validated against experimental data already derived.

2) Measure and correlate mixing efficiency for liquid/gas swirl coaxial element flows similar to the Burick correlation. Since there are little data currently available, this should include an experimental program, although conducting numerical experiments is also recommended as in #1.
3) Extend or improve mixing efficiency correlations for liquid/liquid swirl coaxial element flows.
4) Improve the atomization model for swirled liquid injected from the center orifice of a conventional swirl coaxial element. This improvement is a key need for analyzing swirl coaxial elements for any injector configuration that uses this element.
5) Generate atomization data for swirled liquid injected from the center orifice of a swirl coaxial element, including breakup length data and drop size data. These data will be critical to validating the atomization model described in #4.
6) Improve the atomization model for liquid injected from the outer annulus of a coaxial element. Both axial and swirl injection should be considered. This model will make analysis of the liquid/liquid coaxial element feasible. Predictions from currently available models of this flow are unreliable.
7) Generate atomization data for liquid injected from the outer annulus of a coaxial element, including breakup length data and drop size data. These data will be critical to validating the atomization model described in #6.
8) Ensure that the mixing and atomization data are generated over a wide range to accommodate deep throttling conditions.
9) When conducting hot-fire test programs, extend the tested range of conditions, especially to lower chamber pressures, to generate a wide range of parametric data for improving model capability.

For stability modeling, further development is required to calculate organ pipe resonance frequencies and their responses in the oxidizer posts of swirl coax elements, along with further elucidation of the influence of *d/V*-type instabilities. In addition, with liquid methane, stabilization devices in the combustion chamber will almost certainly be required when such conventional elements and designs are used, so further development of modeling the influences of damping devices will be necessary.

This paper does not include results from calculations with combustion computational fluid dynamic (CFD) models. The authors certainly recognize that future capability with combustion CFD models will eventually overtake the one-dimensional models. However, the mixing and atomization model developments recommended above will be useful (or indeed, critical) in development and validation of combustion CFD models as well.

In the interim before the general use of CFD for complete modeling of performance and stability, CFD models can be used in other ways. Use of CFD to calculate parameters of importance to one-dimensional (non-CFD) modeling has been under development at the NASA MSFC for some time. Recently, calculations of $E_m$ of shear coaxial element flows with $LO_2/gCH_4$ propellants have been conducted using Loci-CHEM. Such calculations can provide significant improvement to one-dimensional model inputs and possible preclude the necessity of measuring such parameters in difficult-to-run experiments.

## Acknowledgments

This activity was funded by the NASA Glenn Research Center under the supervision of Mark Klem and Tim Smith. Sandy Elam of NASA MSFC designed and fabricated all NASA MSFC in-house hardware and planned all tests, while Cynthia Sprader of NASA MSFC conducted all tests. High-frequency planar spectrograms were produced by Jeremy Kenny of NASA MSFC. Thanks to Ross Hewitt of Aerojet General Corporation for further discussions about swirl coax element combustion instability.

## References

[1]Trinh, H., Chapman, J., Elam, S., Jones, G., Robinson, J., Stephenson, D., Hulka, J., and Osborne, R., "Overview of Liquid Oxygen/Liquid Methane Engine Advanced Technology Development at NASA Marshall Space Flight Center," 6th Modeling and Simulation Subcommittee /4th Liquid Propulsion Subcommittee/3rd Spacecraft Propulsion Subcommittee Joint Meeting, Orlando, FL, December 8-12, 2008.

[2]http://spaceflightsystems.grc.nasa.gov/Advanced/Capabilities/PCAD/

[3]Valler, H.W., "Design, Fabrication, and Delivery of a High Pressure LOX-Methane Injector," NASA CR-161343, Aerojet Liquid Rocket Company Report 33205F, Contract NAS8-33205, 15 November, 1979.

[4]Wheeler, D.B., and Kirby, F.M., "High Pressure LOX/CH4 Injector Program, Final Report," NASA CR-161342, Rocketdyne Report 79-278, Contract NAS8-33205, September, 1979.

[5]Bailey, C.R., "High Pressure LOX/Natural Gas Staged Combustion Technology," 1984 JANNAF Propulsion Meeting, New Orleans, LA, February 1984.

[6]Bailey, C.R., "Test Evaluation of Oxygen-Methane Main Injectors," 1987 JANNAF Propulsion Meeting, 1987.

[7]Jensen, R.J., Dodson, H.C., and Claflin, S.E., "LOX/Hydrocarbon Combustion Instability Investigation," NASA CR-182249, Rocketdyne Report RI/RD 89-179, Contract NAS3-24612, July 1989.

[8]Elam, S., Sprader, C., and Parton, J., "Test Report for Test Program P8006B – LOX/GCH4 Technology Demonstration," NASA MSFC TR ET10-09-02, May 12, 2009.

[9]Locke, J.M., Pal, S., and Woodward, R.D., "Chamber Wall Heat Flux Measurements for a LOX/CH4 Uni-element Rocket," AIAA Paper No. 2007-5547, July 2007.

[10]Pierce, C., Trinh, H., Chapman, J., and Elam, S., "Advanced Technology Development of Cryogenic Liquid Oxygen/Methane Engines Relevant to NASA Constellation Systems," 54th JANNAF Propulsion Meeting/3rd Liquid Propulsion Subcommittee Meeting, Denver, CO, May 14-17, 2007.

[11]Engers, R., Balepin, V., Greason, J., and Pierce, C., "Liquid Oxygen/Methane Rocket Engine Development," 54th JANNAF Propulsion Meeting/3rd Liquid Propulsion Subcommittee Meeting, Denver, CO, May 14-17, 2007.

[12]Melcher, J., and Allred, J., "Liquid Oxygen/Liquid Methane Testing of the RS-18 at NASA White Sands Test Facility," AIAA Paper No. 2008-5247, July 2008.

[13]Melcher, J.C., Allred, J.K, and Cabiran, M.L., "Liquid Oxygen/Liquid Methane Testing of the RS-18 Lunar Ascent Engine at Simulated Altitude Conditions at NASA White Sands Test Facility," 6th Modeling and Simulation Subcommittee /4th Liquid Propulsion Subcommittee/3rd Spacecraft Propulsion Subcommittee Joint Meeting, Orlando, FL, December 8-12, 2008.

[14]Robinson, P.J., Veith, E.M., Linne, D.L., and Robinson, J.W., "Design and Development of a 5,500-lbf LOX/LCH4 Ascent Main Engine," 57th JANNAF Propulsion Meeting (JPM) and Joint Meeting of the 7th Modeling & Simulation Subcommittee (MSS) / 5th Liquid Propulsion Subcommittee (LPS) / and 4th Spacecraft Propulsion Subcommittee (SPS), Colorado Springs, CO, May 3-7, 2010.

[15]Elam, S. and Sprader, C., "Test Summary Report for Test Program P2514 – 6 inch LOX/LCH4 Injector Demonstration," NASA MSFC TR ET10-07-01, August 7, 2007.

[16]Elam, S., Protz, C., and Reynolds, D., "Design and Demonstration of a Liquid Oxygen/Liquid Methane (LOX/LCH4) Impinging Injector," 54th JANNAF Propulsion Meeting / 3rd Liquid Propulsion Subcommittee Meeting, Denver, CO, May 14-17, 2007.

[17]Elam, S. and Sprader, C., "Test Report for Test Program P7061 -- LOX/LCH4 Demonstration with Coaxial Injectors," NASA MSFC TR ET10-08-01, July 22, 2008.

[18]Elam, S., and Sprader, C., "Test Report for Test Program P8006A – LOX/LCH4 Technology Demonstration," NASA MSFC TR ET10-09-01, March 18, 2009.

[19]Muss, J.A., "User's Manual for Sierra Engineering's 2006 Version of Rocket Combustor Interactive Design (ROCCID 2006) and Analysis Computer Program," Sierra Engineering, May 2008.

[20]Sutton, R.D., Schuman, M.D., and Chadwick, W.D., "Operating Manual for Coaxial Injection Combustion Model," NASA CR-129031, April 1974.

[21]Luke, E. A., Tong, X.-L., Wu, J. and Cinella, P., "CHEM 2: A Finite-Rate Viscous Chemistry Solver – The User Guide," MSSU-COE-ERC-04-07, Mississippi State University, September, 2004.

[22]Jones, G., Protz, C., Bullard, B., Hulka, J., Santoro, R., Pal, S., Woodward, R.D., and Marshall, W., "Local Heat Transfer Measurements in a LO2/H2 Single Element Combustor," 53rd JANNAF Propulsion Meeting/2nd Liquid Propulsion Subcommittee Meeting, Monterey, CA, December 5-8, 2005.

[23]Hulka, J., Jones, G., Protz, C., Bullard, B., Trinh, H., Santoro, R., Pal, S., Woodward, R.D., and Marshall, W., "Local Combustion Chamber Heat Flux Measurements with $LO_2/H_2$ Swirl Coaxial Injectors," 54th JANNAF Propulsion Meeting/3rd Liquid Propulsion Subcommittee Meeting, Denver, CO, May 14-17, 2007.

[24]Jones, G., Protz, C., Bullard, B., and Hulka, J., "Local Heat Flux Measurements with Single Element Coaxial Injectors," AIAA Paper No. 2006-5194, July 2006.

[25]"JANNAF Rocket Engine Performance Prediction and Evaluation Manual," CPIA Publication 246, April 1975.

[26]Rupe, J.H., "The Liquid Phase Mixing of a Pair of Impinging Streams," Progress Report No. 20-195, Jet Propulsion Laboratory, Pasadena, CA, August 6, 1953.

[27]Ito, J.I., and Calhoon, D.F., "Investigation of Gaseous Propellant Combustion and Associated Injector/Chamber Guidelines," NASA CR-121234, 1973.

[28]Schuman, M.D., and Beshore, D.G., "Standard Distributed Energy Release (SDER) Computer Program, Final Report, Volume I," AFRPL-TR-78-7, August 1978.

[29]Nurick, W.H., "DROPMIX – a PC-Based Program for Rocket Engine Injector Design," JANNAF Combustion Meeting, Cheyenne, WY, Nov. 1990.

[30]Burick, R.J., "Space Storable Propellant Performance Program Coaxial Injector Characterization," NASA CR-120936, Rocketdyne Report No. R-8973-2, Oct. 1972.

[31]Hulka, J., and Schneider, J.A., "Single Element Injector Cold Flow Testing for STME Swirl Coaxial Injector Element Design," AIAA Paper No. 93-2161, June 1993.

[32]Aithal, S.M., Liu, Z., Jensen, R.J., Hinerman, T.D., and Lynch, E.D., "Nonlinear Injection Transfer Function Simulations for Liquid Propellants," AIAA Paper No. 2008-4742, July 2008.

[33]Rupe, J.H., "A Correlation Between the Dynamic Properties of a Pair of Impinging Streams and the Uniformity of Mixture-Ratio Distribution in the Resulting Spray," Progress Report No. 20-209, Jet Propulsion Laboratory, Pasadena, CA, March 28, 1956.

[34]Anderson, W.E., Ryan III, H.M., Santoro, R.J., and Hewitt, R.A., "Combustion Instability Mechanisms in Liquid Rocket Engines Using Impinging Jet Injectors," AIAA Paper No. 95-2357, July 1995.

[35]Hewitt, R.A., "Combustion Instability in Liquid Rockets (with a d/V Correlation Perspective)," invited lecture delivered at the 42nd AIAA/ASME/SAE/ASEE Joint Propulsion Conference, Sacramento, CA, July 10, 2006.

[36]Wenzel, L.M., and Szuch, J.R., "Analysis of Chugging in Liquid-Bipropellant Rocket Engines Using Propellants with Different Vaporization Rates," NASA TN D-3080, October 1965.

[37]Hulka, J.R, "Combustion Instability of Swirl Coaxial Element Injectors with Liquid Oxygen/Liquid Methane Propellants," 57th JANNAF Propulsion Meeting (JPM) and Joint Meeting of the 7th Modeling & Simulation Subcommittee (MSS) / 5th Liquid Propulsion Subcommittee (LPS) / and 4th Spacecraft Propulsion Subcommittee (SPS), Colorado Springs, CO, May 3-7, 2010.

[38]*Guidelines for Combustion Stability Specification and Verification Procedures for Liquid Propellant Rocket Engines*, M.D. Klem and R.S. Fry, editors, CPIA Publication 655, Jan. 1997.

[39]Anon., "4400-Hz Vibration Investigation, Final Report," Rocketdyne Report R-8742, Contract NAS8-25156, Canoga Park, CA, June 30, 1971.

[40]Hutt, J.J., and Rocker, M., "High-Frequency Injection-Coupled Combustion Instability," Chapter 12, Liquid Rocket Engine Combustion Instability, V. Yang and W. Anderson, editors, Progress in Astronautics and Aeronautics, Vol. 169, 1995, pp. 345-355.

[41]Bazarov, V., Yang, V., and Puri, P., "Design and Dynamics of Jet and Swirl Injectors," Liquid Rocket Thrust Chambers: Aspects of Modeling, Analysis, and Design, V. Yang, M. Habiballah, J. Hulka, and M. Popp, editors, Progress in Astronautics and Aeronautics, Vol. 200, 2004, pp. 19-103.

[42]Hulka, J., and Hutt, J.J., "Instability Phenomena in Liquid Oxygen/Hydrogen Propellant Rocket Engines," Chapter 2, Liquid Rocket Engine Combustion Instability, V. Yang and W. Anderson, editors, Progress in Astronautics and Aeronautics, Vol. 169, 1995, pp. 39-71.

[43]Muss, J.A., "Instability Phenomena in Liquid Oxygen/Hydrocarbon Rocket Engines," Chapter 3, Liquid Rocket Engine Combustion Instability, V. Yang and W. Anderson, editors, Progress in Astronautics and Aeronautics, Vol. 169, 1995, pp. 73-88.

[44]Hulka, J.R., Hewitt, R.A., Grissom, W.M., Hart, G.L., Kopicz, C.F., and Shadoan, M.D., "Combustion Stability and Performance of Subscale $LO_2/LH_2$ Preburners for COBRA Engine Development," 52nd JANNAF Propulsion Meeting / 1st Liquid Propulsion Subcommittee Meeting, Las Vegas, NV, May 1-5, 2004.

[45]Doumas, L., and Laster, R., "Liquid-Film Properties for Centrifugal Spray Nozzles," Chemical Engineering Progress, Vol. 49, No. 10, October 1953.

[46]Im, J.-H., Kim, D., Yoon, Y., Roh, T.-S., and Koo, J.-Y., "Self-Pulsation Characteristics of a Swirl Coaxial Injector with Various Injection and Geometric Conditions," AIAA Paper No. 2005-3749, July 2005.

[47]Cha, E., Kim, D., Kim, B.S., Yoon, Y., and Bazarov, V. "Analysis of Swirl Coaxial Injector with Backhole as an Acoustic Damper in Liquid Rocket Engines," AIAA Paper No. 2005-3748, July 2005.




# Performance and Stability Analyses of Rocket Thrust Chambers With Oxygen/Methane Propellants

**Gregg Jones**, NASA MSFC

**Jim Hulka**, Jacobs Engineering, ESTS Group

Huntsville, AL

# Motivation – Technology Development of $LO_2/CH_4$ LRE Combustion Devices

- NASA considering use of oxygen and methane propellants for future in-space missions
  - Improves performance over storable propellants
  - Provides compatible oxidizer (oxygen) with life support systems
  - Provides possibility for *in-situ* propellant production
- Oxygen-methane propellants are not used on any current flight-qualified space propulsion system
- Significant increase in Technology Readiness Level (TRL) of thrust chamber technology is required
  - Capability to analyze thrust chamber phenomena
    - Combustion, performance, heat transfer, stability, ignition

# Objectives of NASA Combustion Devices Analysis Plans

- Long Term:
  - Improve and validate capability to analyze multi-element thrust chamber combustion with oxygen and methane propellants
    - Performance
    - Combustion Stability
    - Heat transfer
    - Transients
- Near Term:
  - Evaluate current capability to analyze combustion, performance heat transfer, and stability
    - $LO_2/gCH_4$
    - $LO_2/LCH_4$
    - Single element injectors
    - Multi-element injectors

# Evaluate Capability to Predict Combustion, Performance, and Heat Transfer

- Task 1 – Collect information for several test cases
  - Penn State/CUIP LOX/gCH4 single element coax (2006)
    - Shear coax - recessed oxidizer post
    - Shear coax - flush oxidizer post
    - Swirl coax – flush oxidizer post
  - Rocketdyne LOX/gCH4 82-element shear coax (1989)
  - NASA MSFC LOX/LCH4 40-element like-on-like paired doublet (2007)
  - NASA MSFC LOX/LCH4 28-element swirl coax (2008)
  - NASA MSFC LOX/LCH4 40-element swirl coax (2008, 2009)

- Task 2 – Analyze all cases with heritage 1-D codes:
  - Rocket Combustor Interaction Design and Analysis (ROCCID)
  - Coaxial Injector Combustion Model (CICM)

- Task 3 – Analyze progression of cases with combustion CFD
  - Loci-CHEM
  - Not discussed in this paper

# Penn State University/CUIP LOX/gCH4 Single-Element Coax Injectors

Marshall Space Flight Center

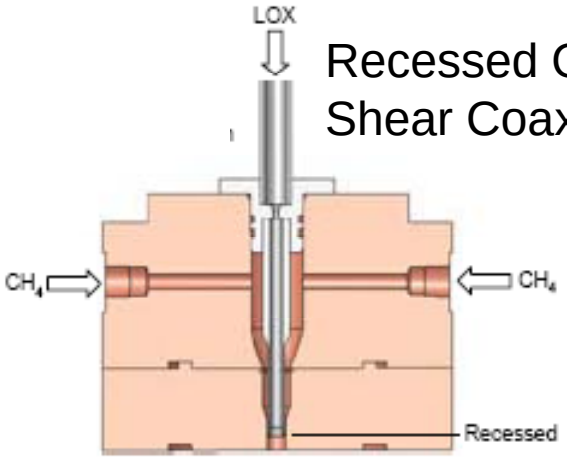


Recessed Oxidizer Post
Shear Coax Injector

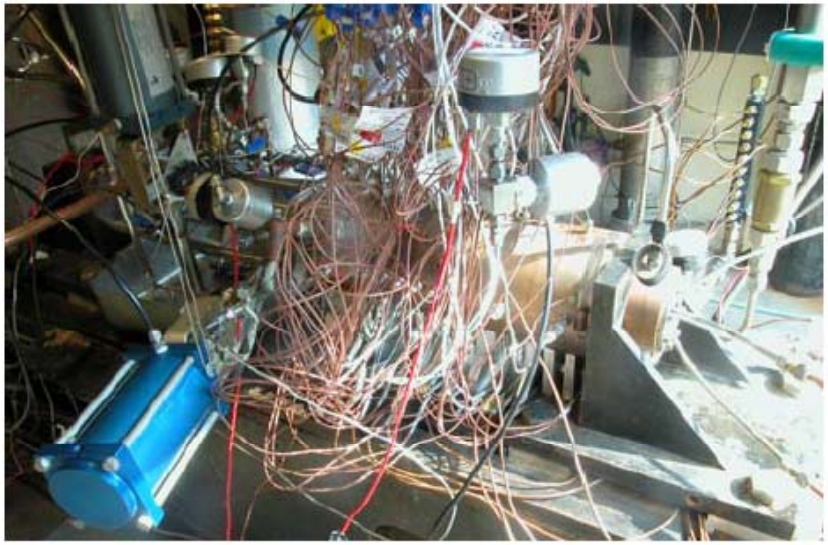

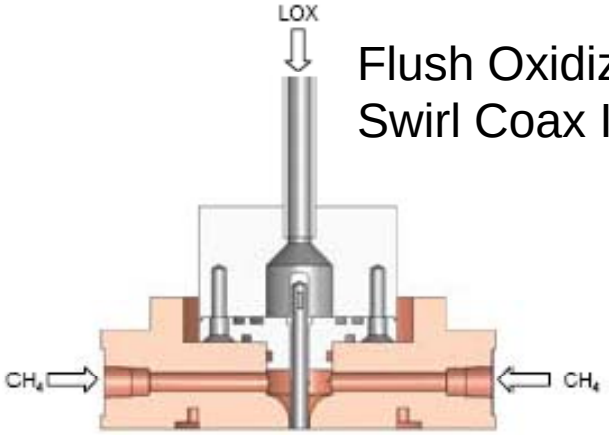


Flush Oxidizer Post
Swirl Coax Injector

Combustion Chamber

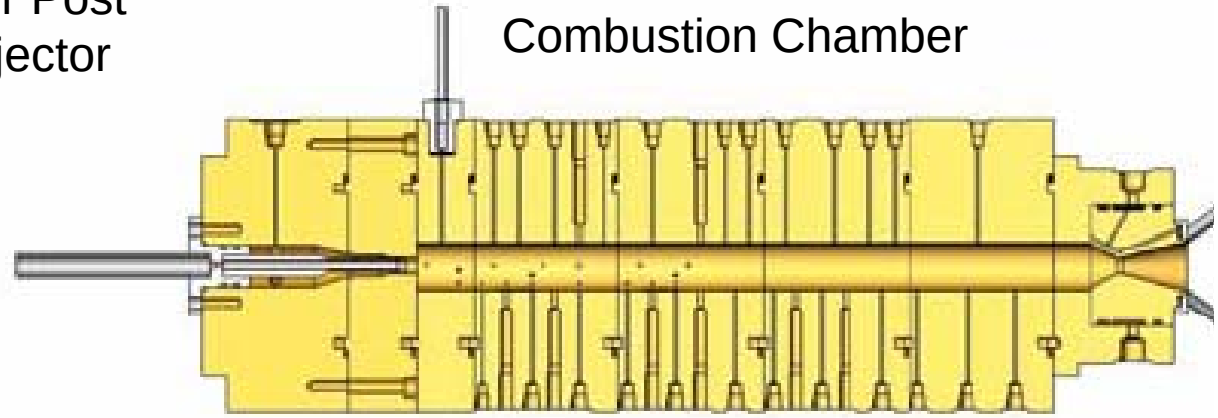

Locke, J.M., Pal, S., and Woodward, R.D., "Chamber Wall Heat Flux Measurements for a LOX/CH4 Uni-element Rocket," AIAA 2007-5547, July 2007.

JACOBS ESTS Group

# PSU CUIP LO2/gCH4 Single-Element Tests
## Measured Relative Performance

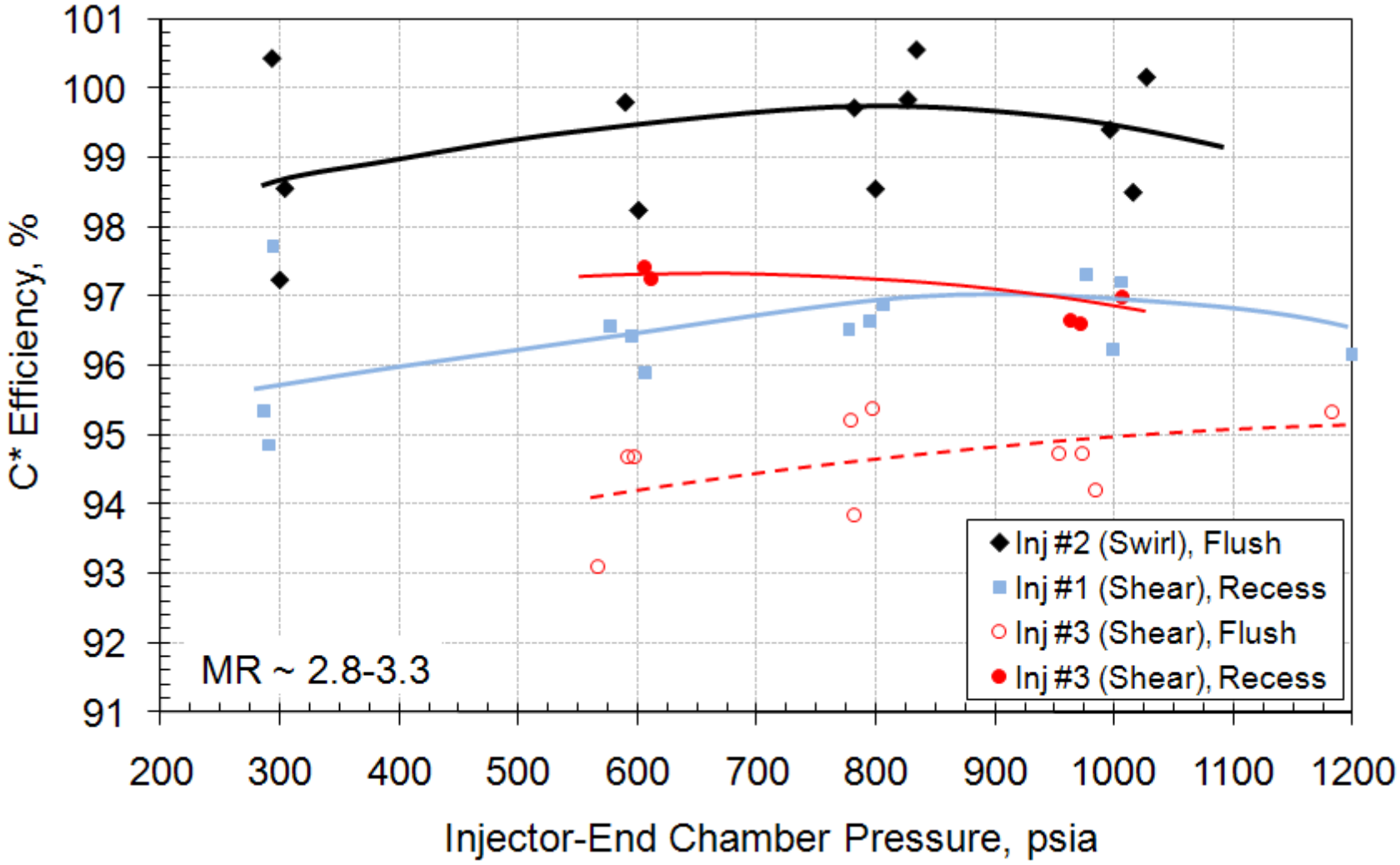

# One-dimensional Combustion Models

- Rocket Combustor Interactive Design and Analysis Program (ROCCID)
  - Developed at Aerojet for NASA GRC in 1991
  - Commercial version currently available from Sierra Engineering
  - Capable of evaluating many element types
    - like-on-like doublets, shear coax, swirl coax (gas and liquid fuels)
  - Steady–State Combustion Iteration (SSCI)
    - Propellant atomization calculated from mechanistic models but atomization parameters can be altered by user
    - Vaporization calculated with Priem & Heidmann Generalized Length correlation
    - Mixing calculated using two-zone four-streamtube model
- Coaxial Injection Combustion Model (CICM)
  - Developed at Rocketdyne for NASA MSFC in 1974
  - JANNAF-standard computer program for evaluation of liquid rocket engine performance
  - Capable of analyzing shear coaxial elements only
  - Steady-state combustion routine
    - Calculates rate of atomization from shear force between jet and surrounding gas
      - Calculates an axially varying mean droplet size
      - Does not require experimental dropsize correlations but does require user-defined parameters
    - Specially developed droplet heating and vaporization model
    - Provides significant mechanistic calculations of combustion in the recessed oxidizer post region – the "cup"
    - Intra-element mixing (*Em*) defined by user – run and average multiple runs at different mixture ratios
      - Then interface with a Distributed Energy Release (DER) or Streamtube Combustion (STC) code

# Methane Shear Coax Elements Out of Range of Burick Liquid/Gas $E_m$ Mixing Correlation

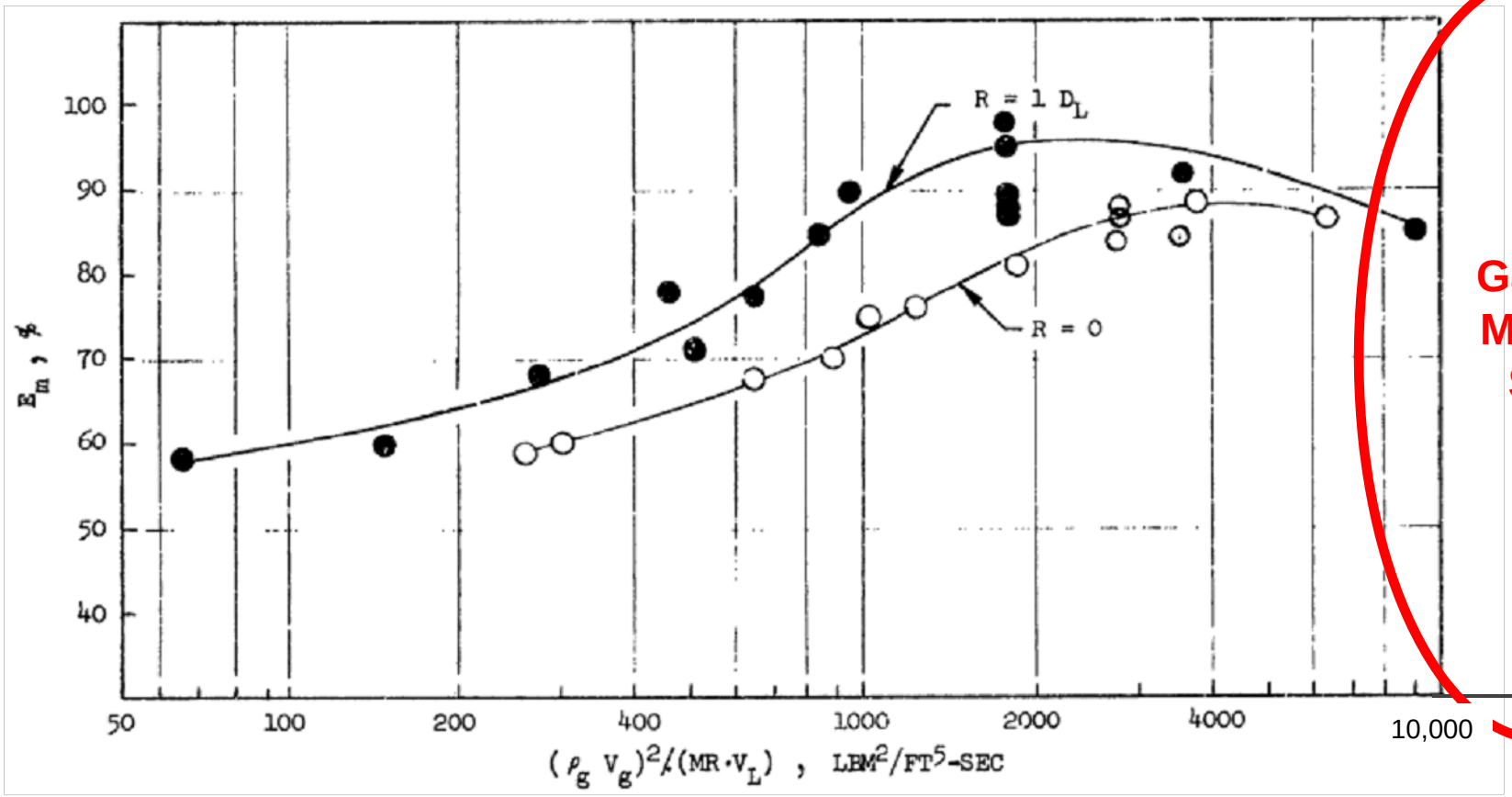


**Gaseous Methane Shear Coax**

# 2008 ROCCID Calculation - Recessed-Post Single-Element Shear Coax

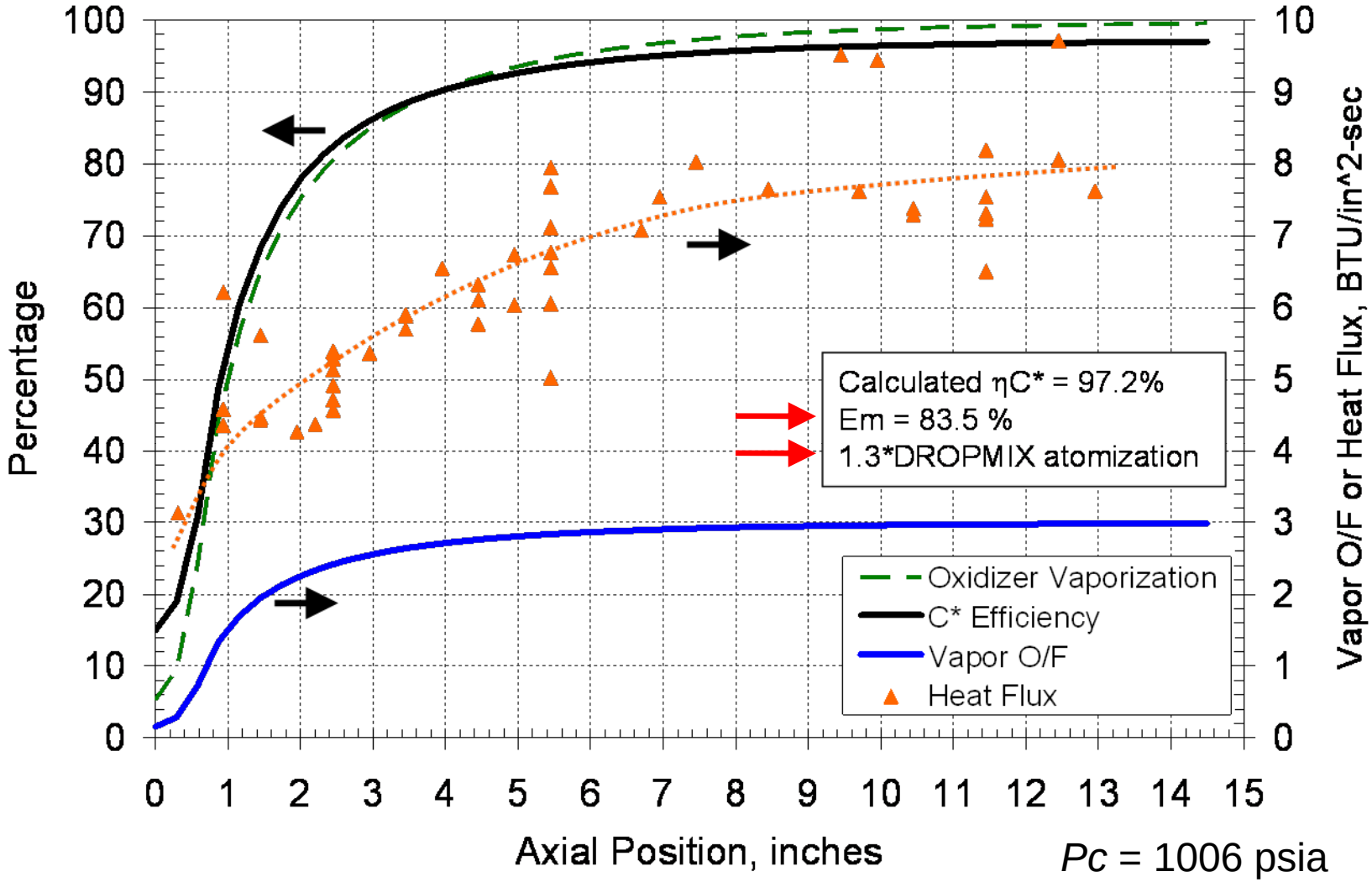


*Pc* = 1006 psia
*MR* = 3.00

# ROCCID Calculation of PSU Shear Coax at *Pc*~300 psia Has Uncertainties

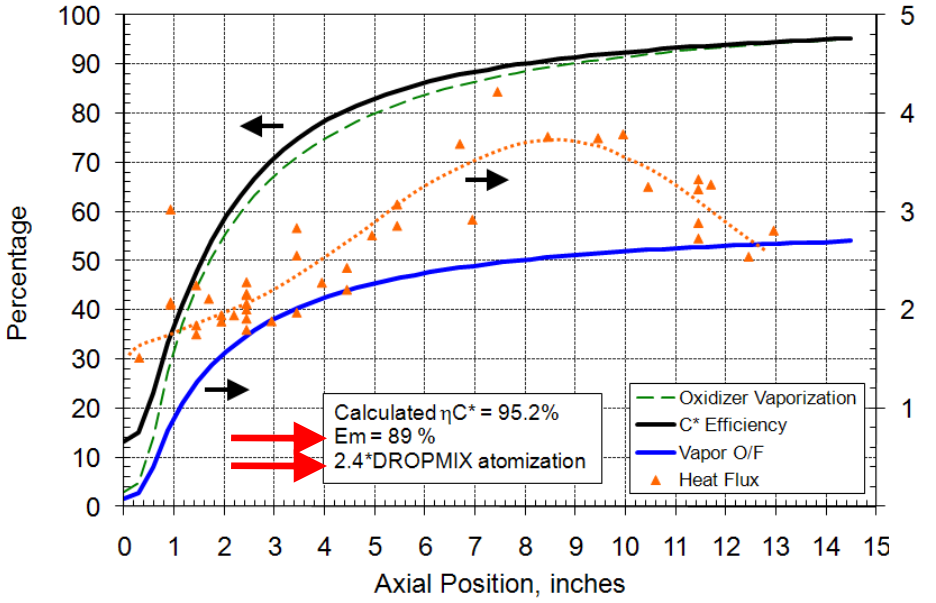


- Very good mixing (from Burick)
- … have to use poor atomization

?

*Pc* = 291 psia
*MR* = 2.84

Good atomization (from DROPMIX) -
… have to use very poor mixing -

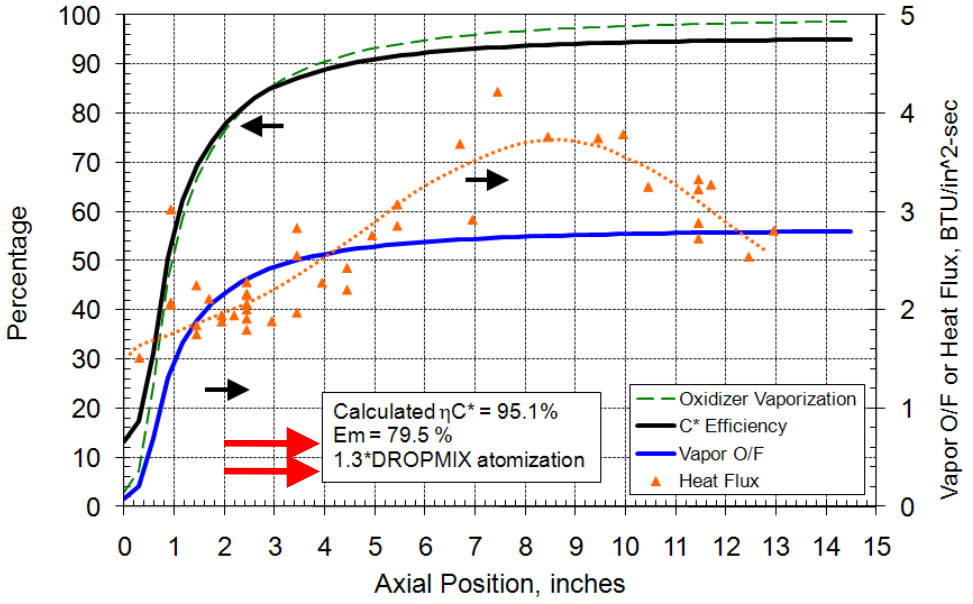

# With New $LO_2/gCH_4$ Atomization Parameters, CICM OK at High Pc But Not Good at Low Pc

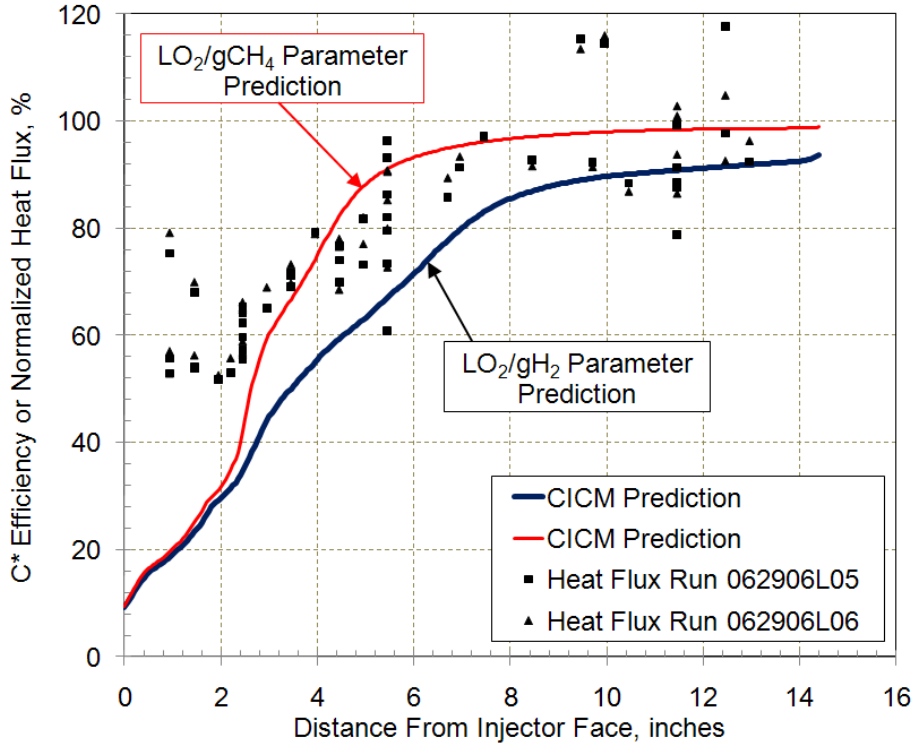


*Pc* = 1006 psia
*MR* = 3.00

**Could not use recommended methods – no measureable cup $\Delta P$ with methane**

*Pc* = 291 psia
*MR* = 2.84

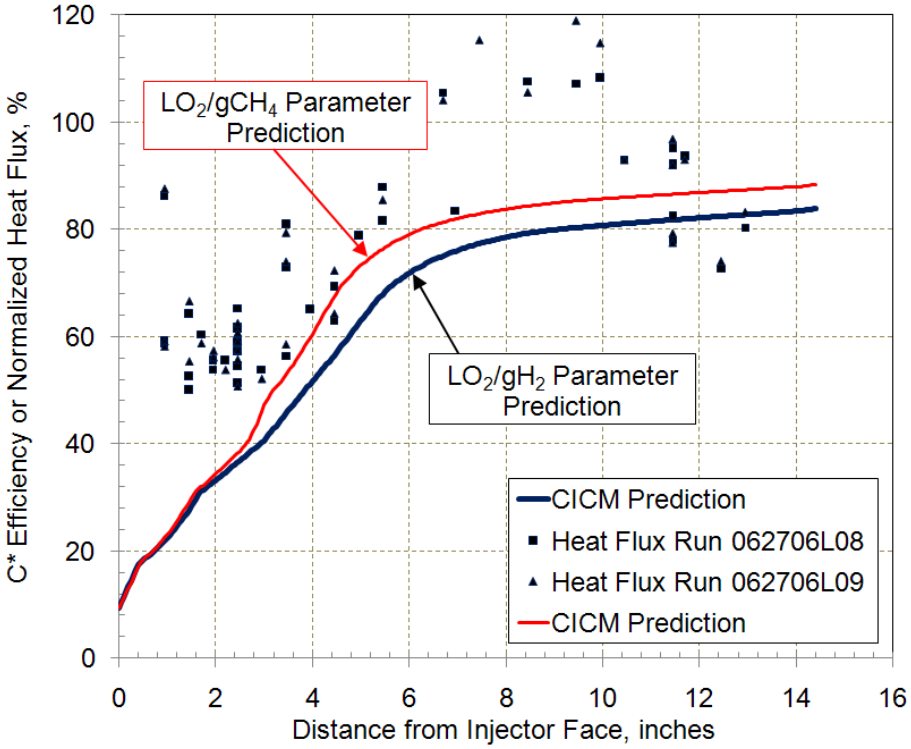

# NASA MSFC Conducted Combustor Testing with $LO_2/LCH_4$ Propellants For Several Years

*Marshall Space Flight Center*

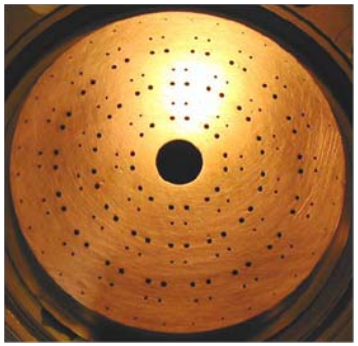

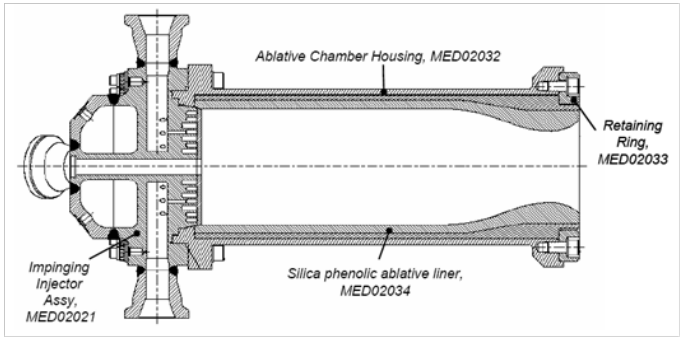


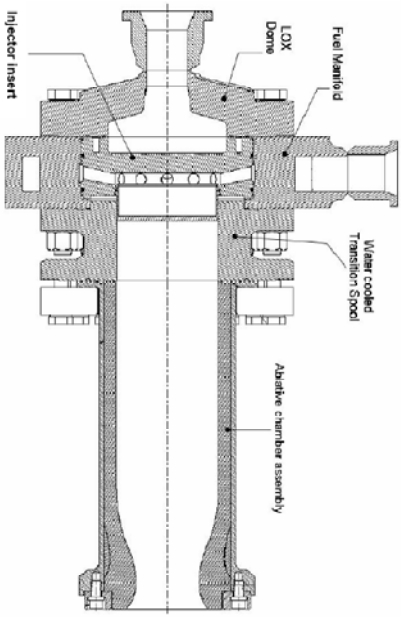


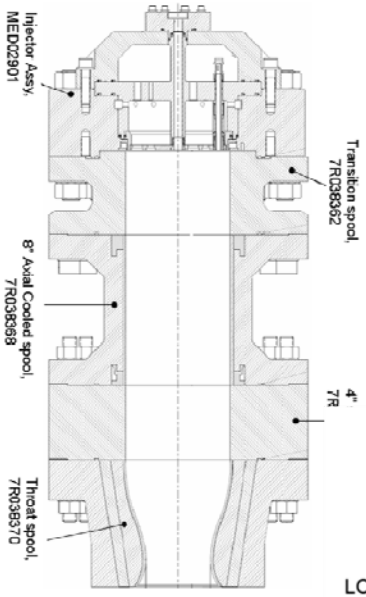



1. Elam, S., and Sprader, C., "Test Summary Report for Test Program P2514 – 6 inch LOX/LCH4 Injector Demonstration," NASA MSFC TR ET10-07-01, August 7, 2007.

2. Elam, S., and Sprader, C., "Test Report for Test Program P7061 – LOX/LCH4 Demonstration with Coaxial Injectors," NASA MSFC TR ET10-08-01, July 22, 2008.

3. Elam, S., and Sprader, C., "Test Report for Test Program P8006A – LOX/LCH4 Technology Demonstration," NASA MSFC TR ET10-09-01, March 18, 2009.


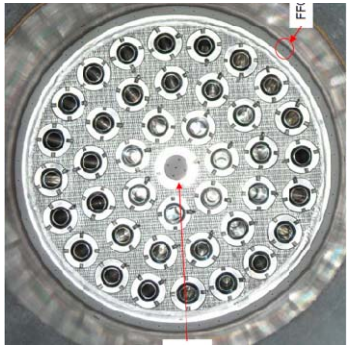

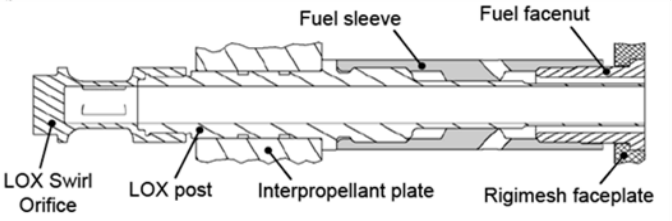


JACOBS ESTS Group

# LCH4/LOX ROCCID Calculation with Like-on-Like Paired Doublet Multi-element Injector is Good

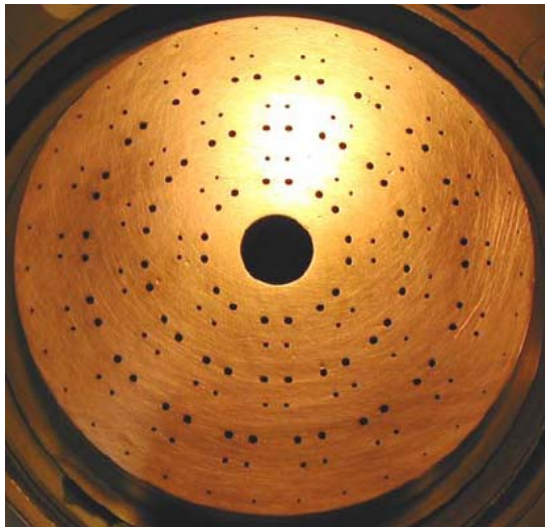

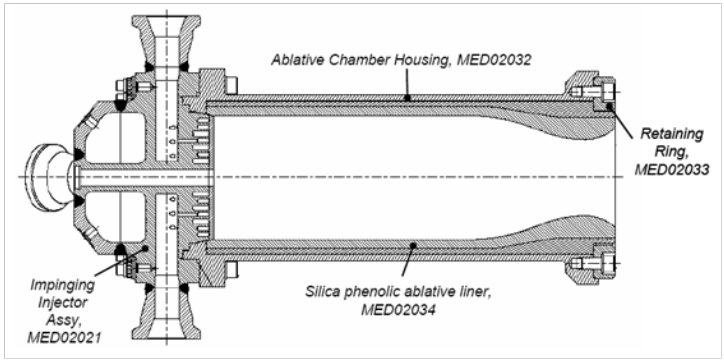


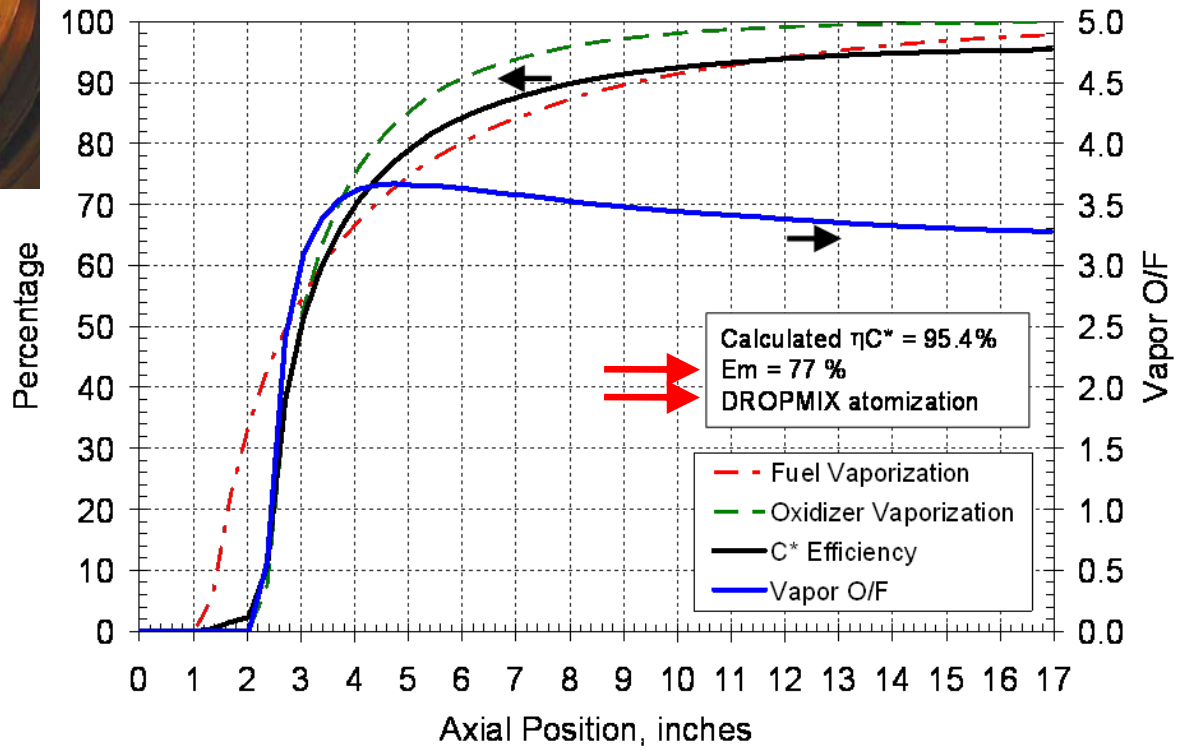

# 28 Element ROCCID Calculation of Performance Change with *L'* is Reasonable

Marshall Space Flight Center

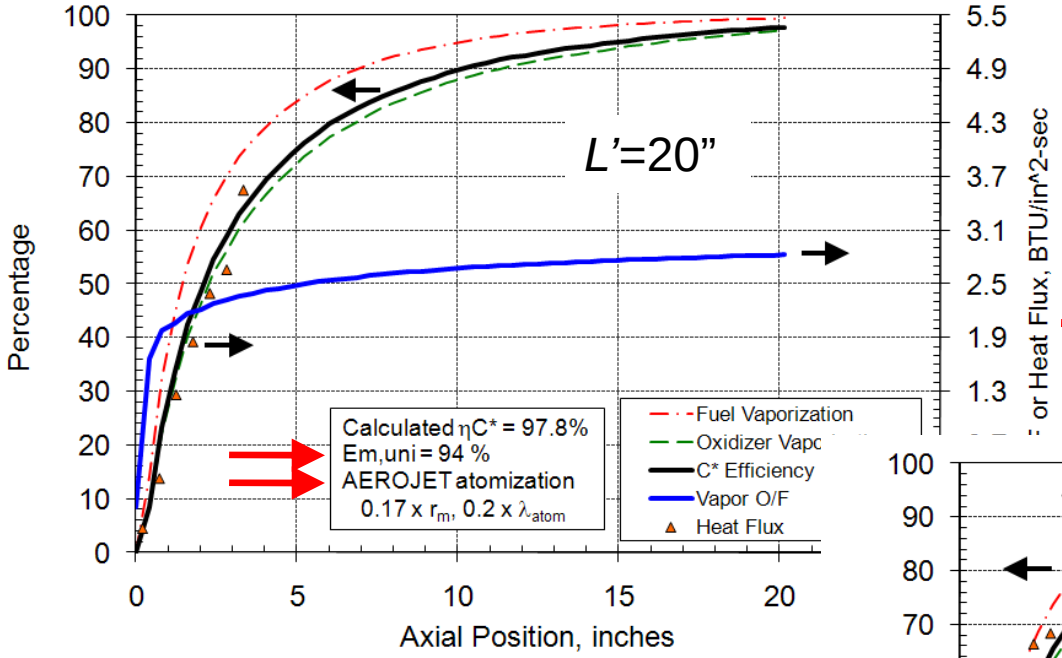


**1.9%** increase in measured $\eta_{c^*}$ from extra 4" of *L'* …

…. due to improvement in vaporization efficiency (**1.5%** shown)

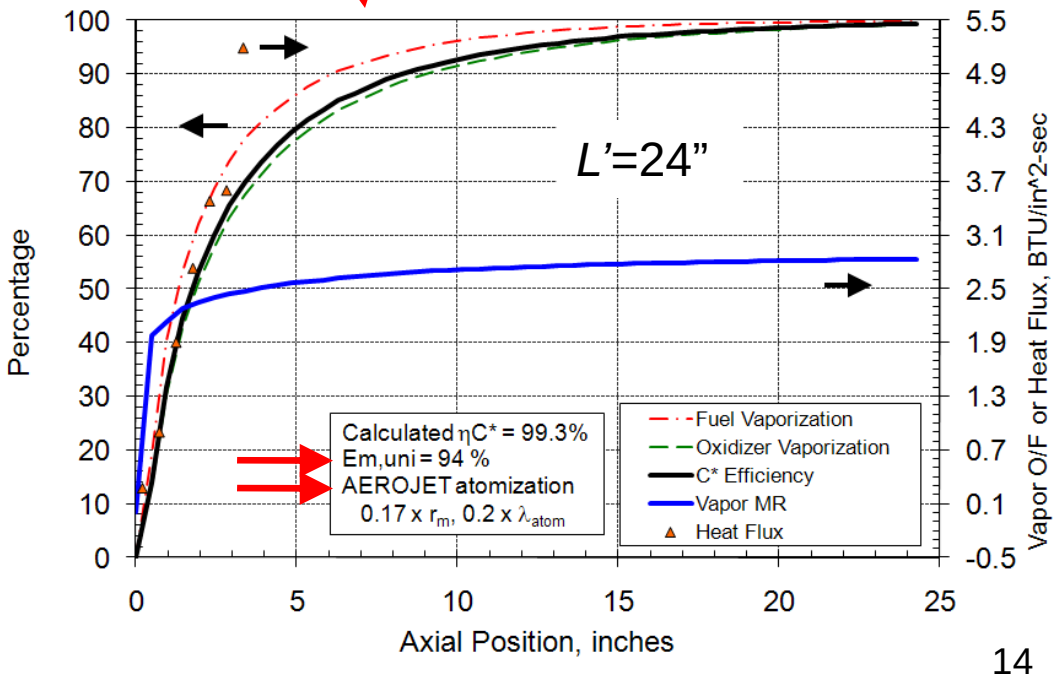


Mass median droplet diameter ~ 190-250 microns

JACOBS ESTS Group

# User-Inputs for Atomization of 28 Element Liquid/Liquid Swirl Coax with Small Fuel Annulus Gaps

*Marshall Space Flight Center*

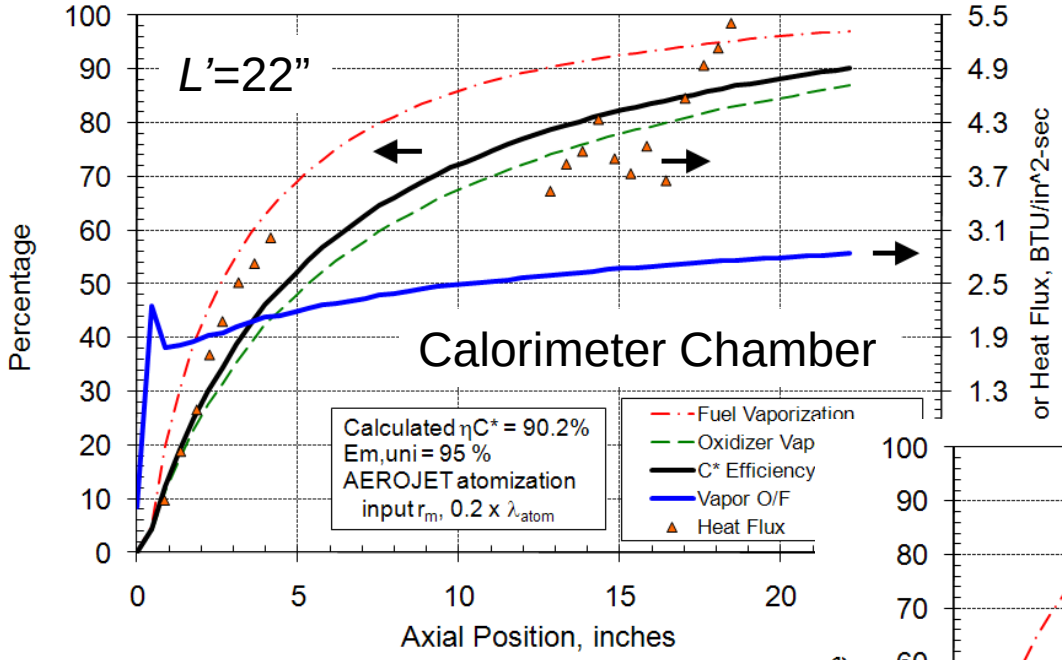


Fuel annulus gap width = large

Mass median droplet diameters ~ 400 microns (F), 450 microns (O)

Fuel annulus gap width = small

Mass median droplet diameters ~ 100 microns (F), 280 microns (O)

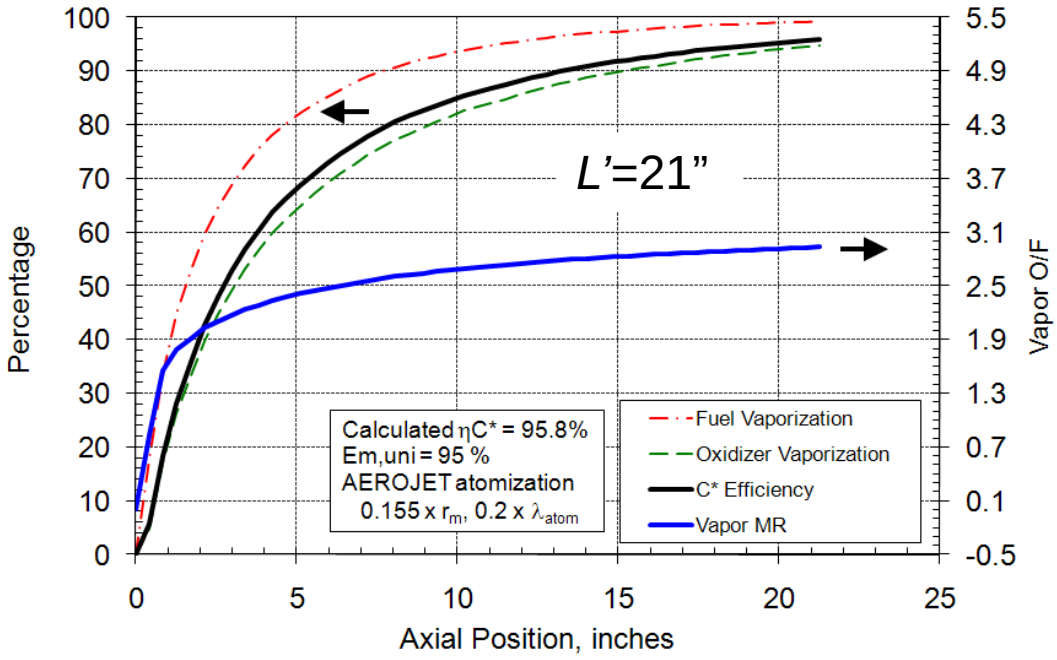


JACOBS ESTS Group

# Chug Waveform with 28-Element Injector Contained Lots of High-Frequency Content

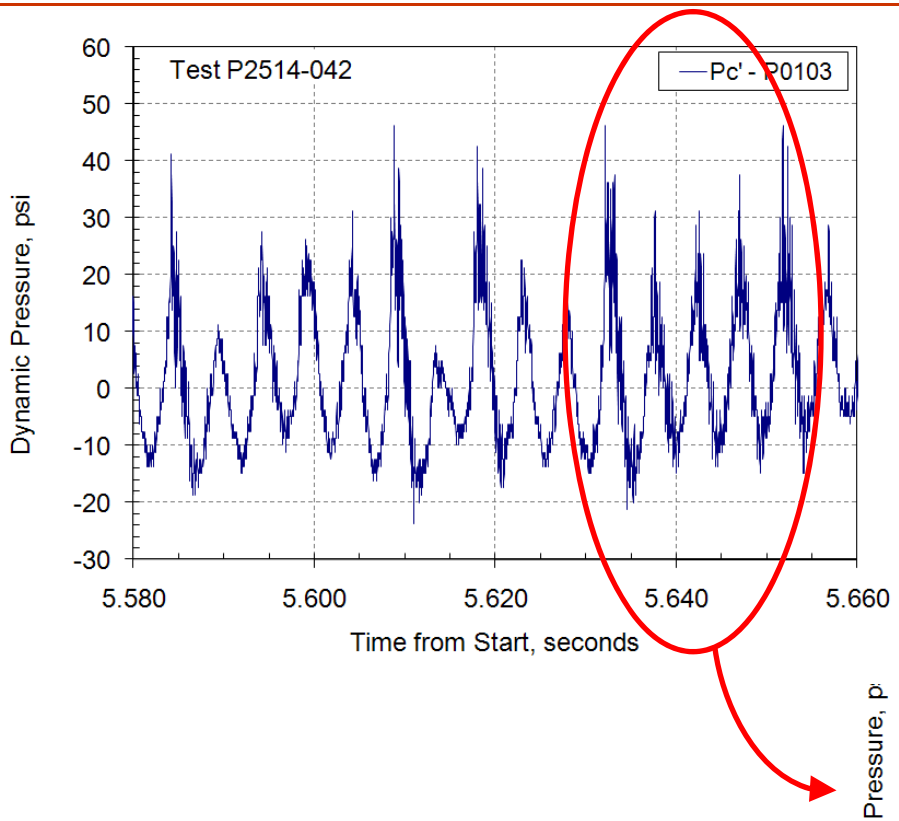


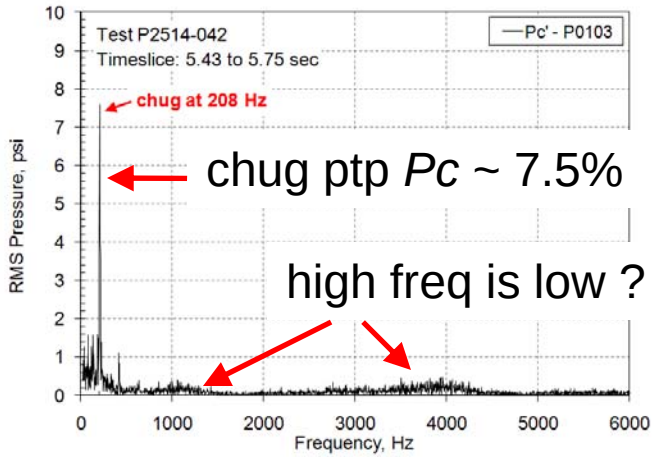


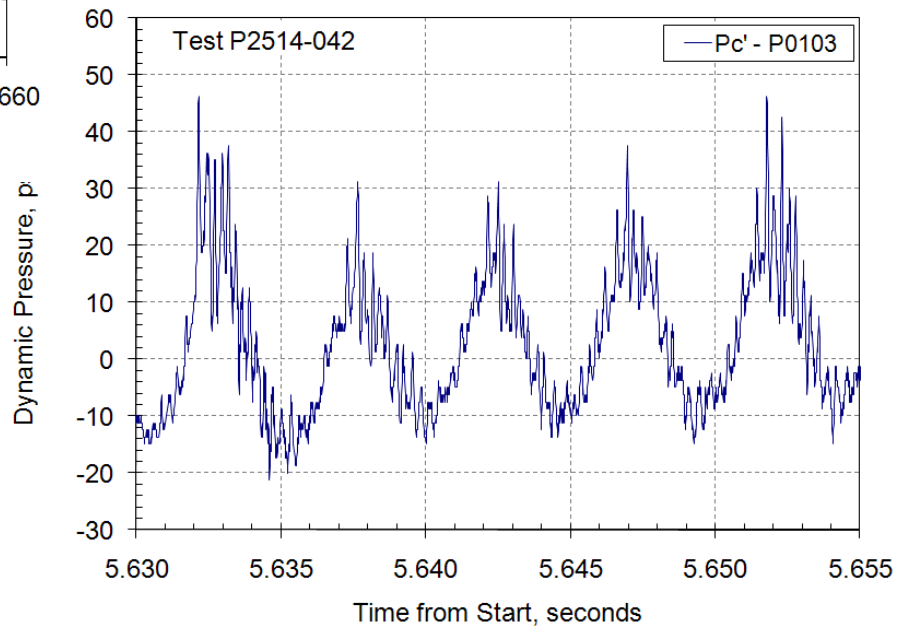

# Oscillations at 2500 Hz May Be Exciting 1T Mode

- Closer look shows extended high frequency oscillation periods
  - some more than “allowable” for acoustic modes

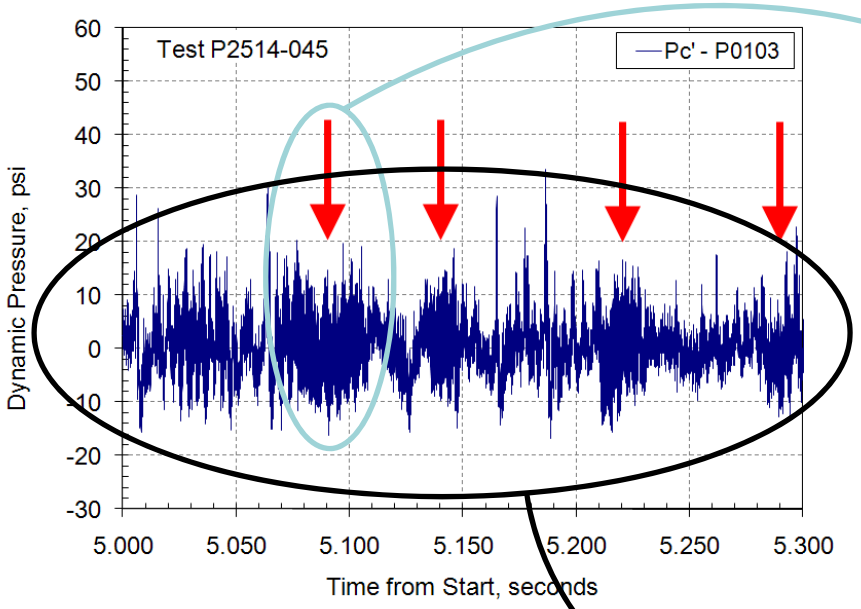


Short duration average spectrum

Long duration average spectrum

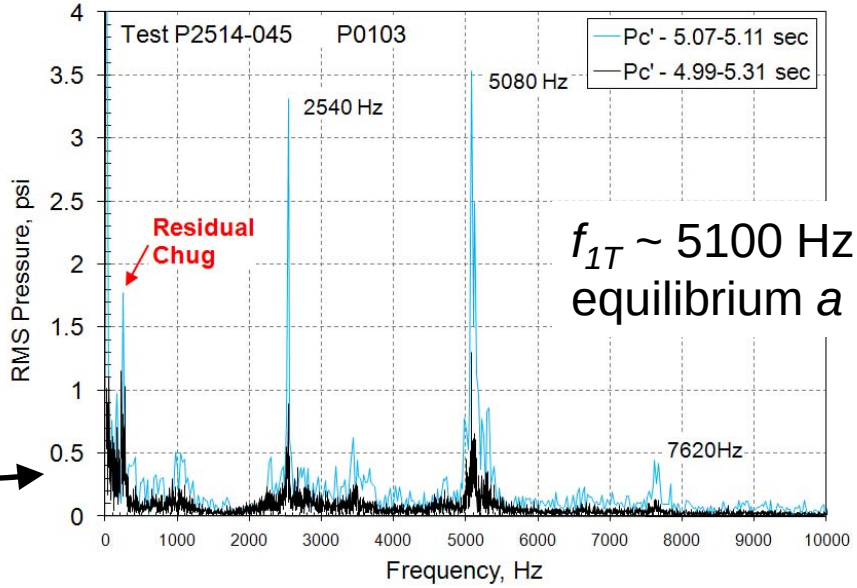


$f_{1T}$ ~ 5100 Hz equilibrium *a*

# Chug Waveform with Initial 40-Element Injectors Also Sporadic with High-Frequency Content



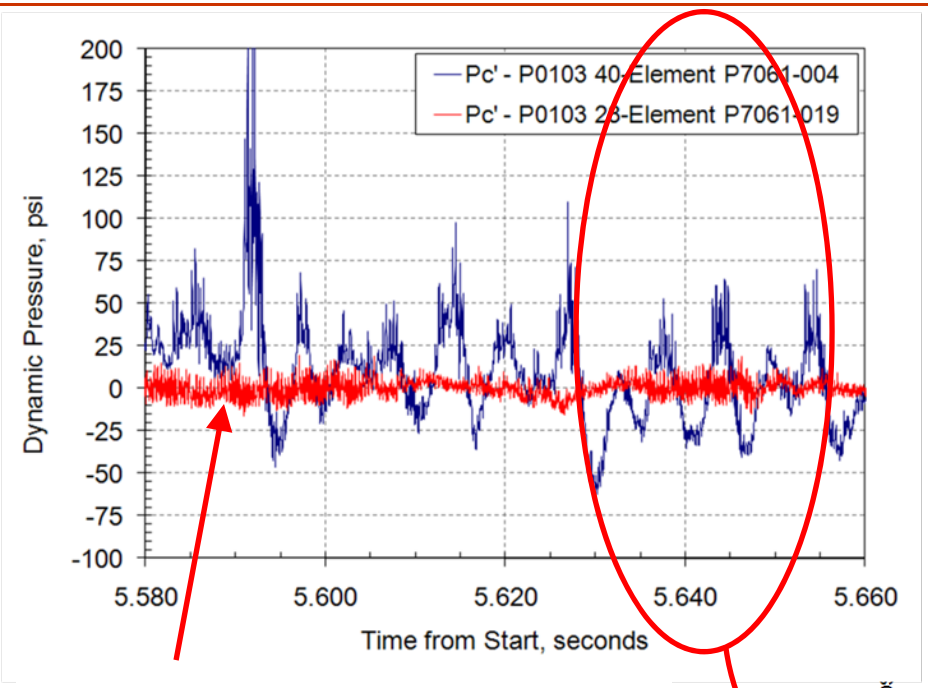


28-element test at same *Pc* and *MR*

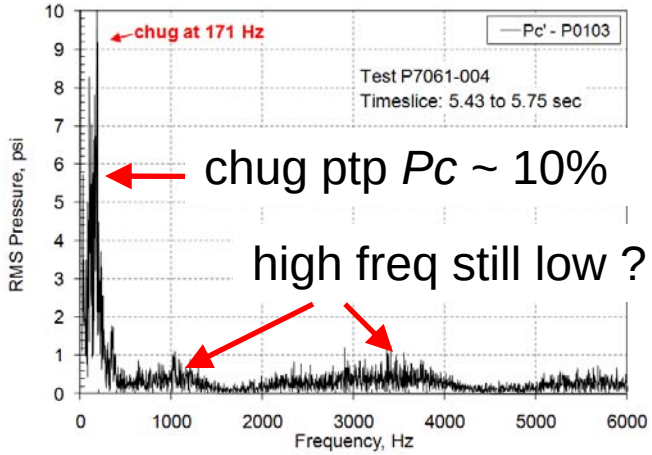


chug ptp *Pc* ~ 10%

high freq still low ?

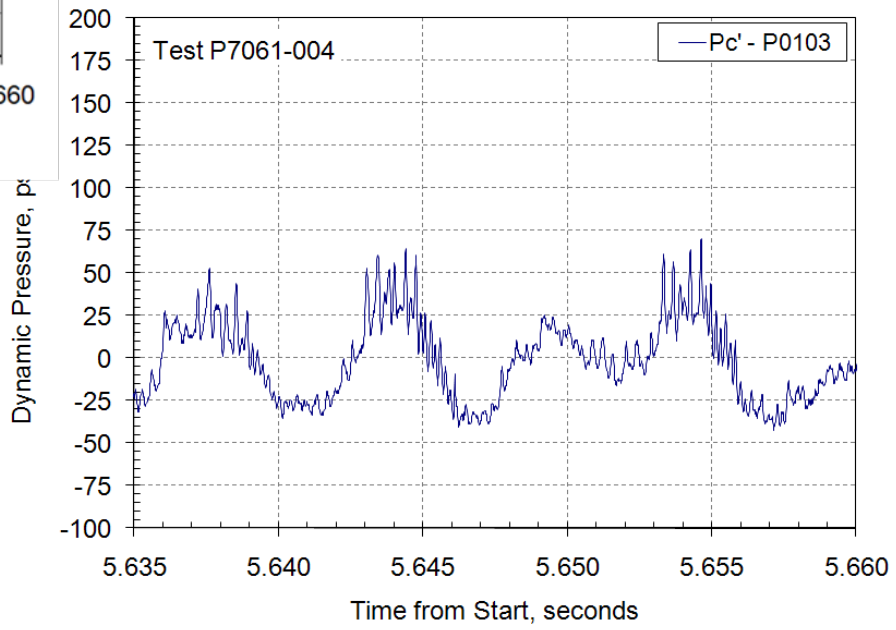

# Damage at Oxidizer Swirl Inlets Was Observed

Damage only to elements in center rows

Cause of damage not yet determined

# … High-Frequency Instability Initiated

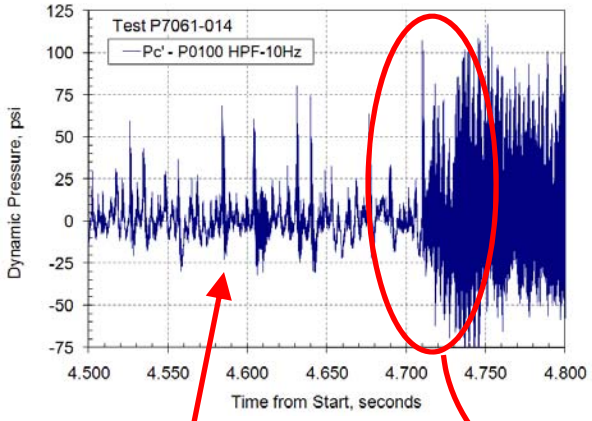


chug at 210 Hz

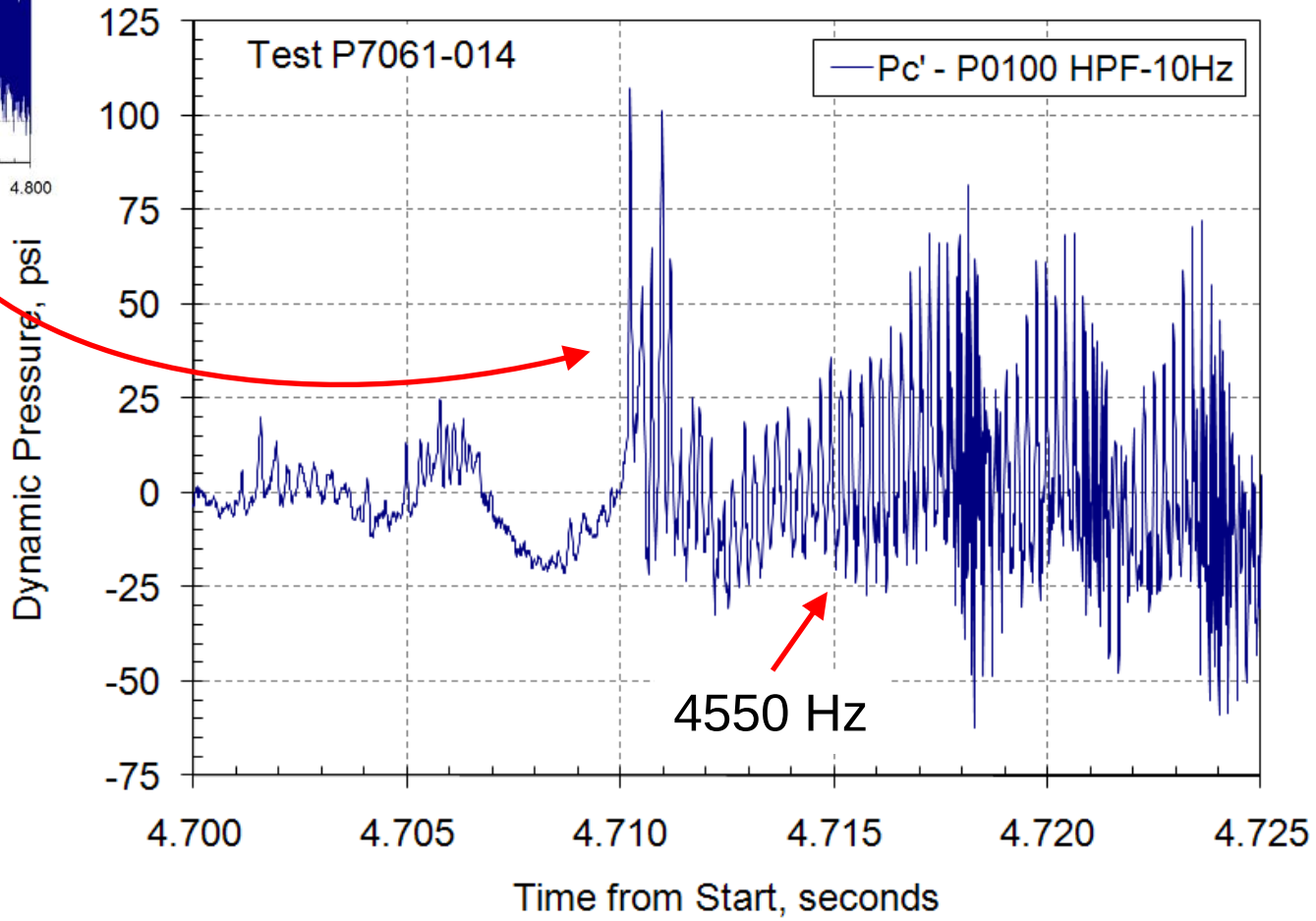

# Transition from Chug at 210 Hz to High-Frequency at 4550 Hz

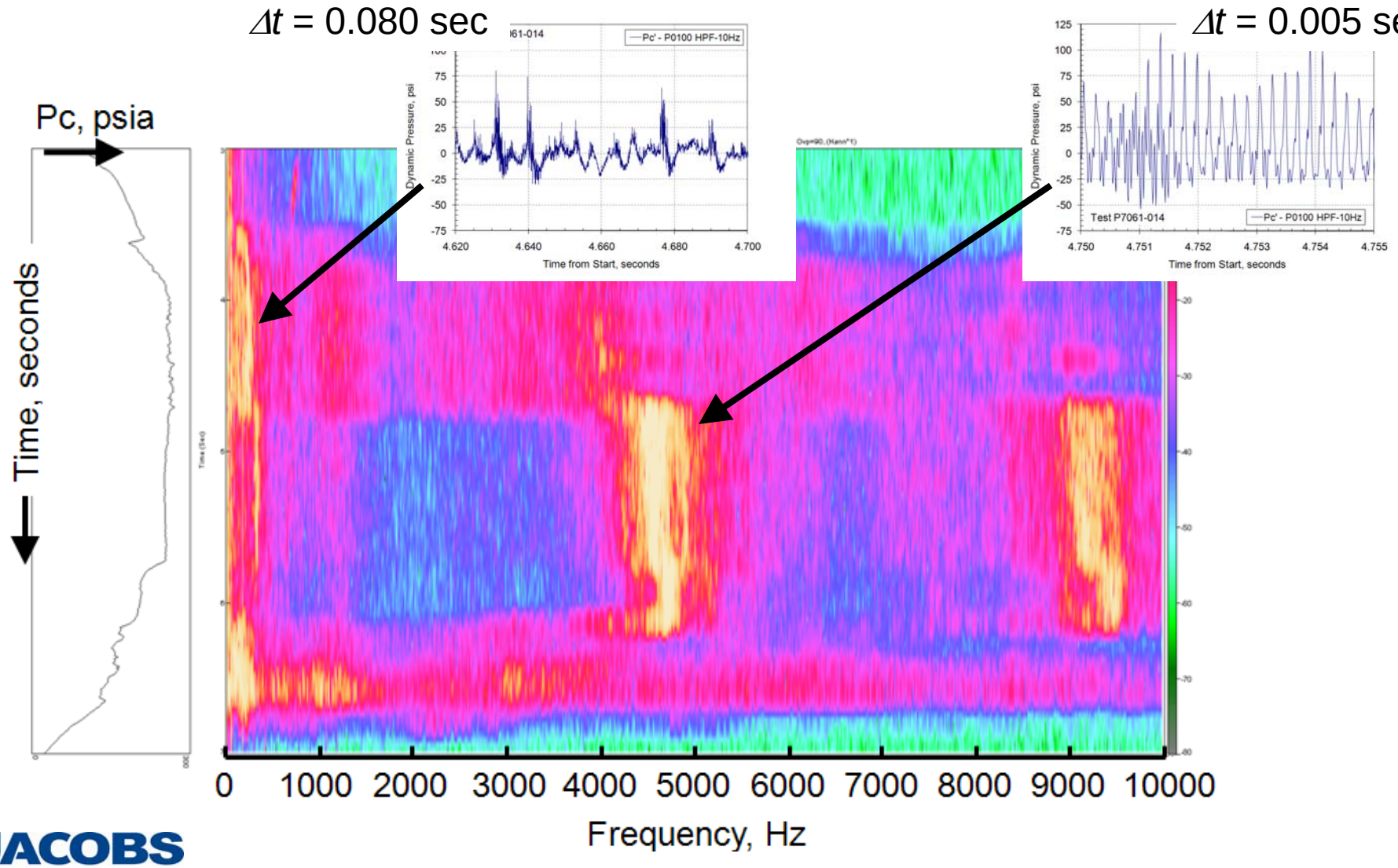

# High-Frequency Instability Occurred Again In Calorimeter Chamber



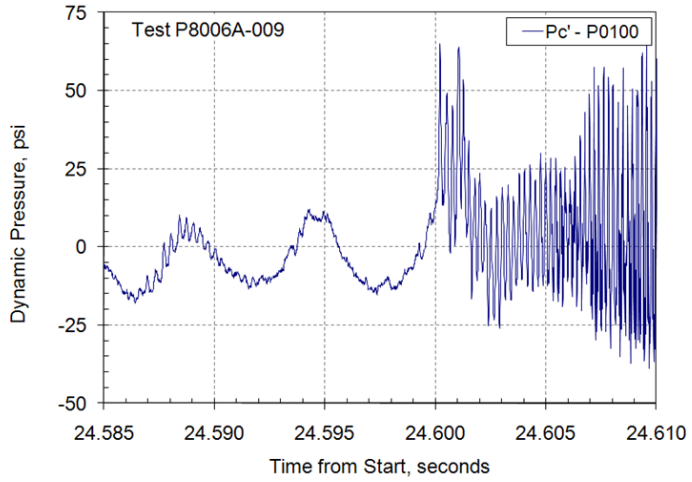


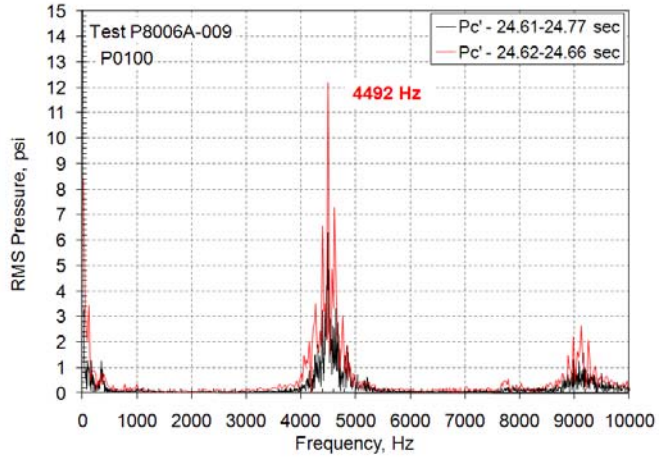


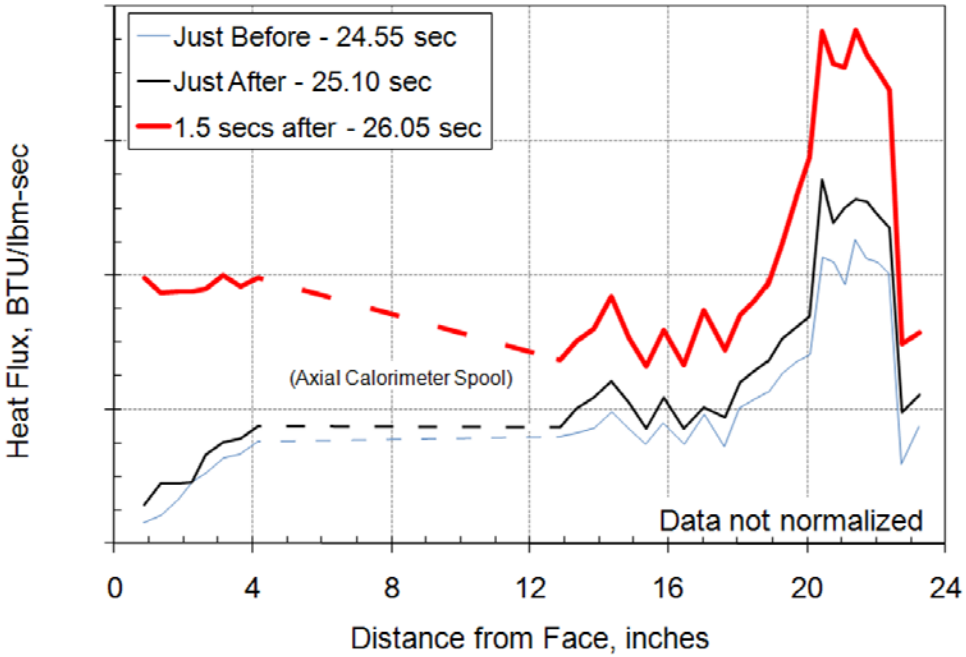


- 4490 Hz is 89% of equilibrium $f_{1T}$
- Factor of 11 increase in head-end heat flux
- Factor of 1.8 increase in throat heat flux

…very likely the 1T mode

# 4000 Hz and 5000 Hz Oscillations may be from Hewitt *"d"/V*

- Hewitt Stability Correlation for "unlike doublets"
  - Use for unlike propellant impingent
  - "Twice as unstable" as like-on-like doublets

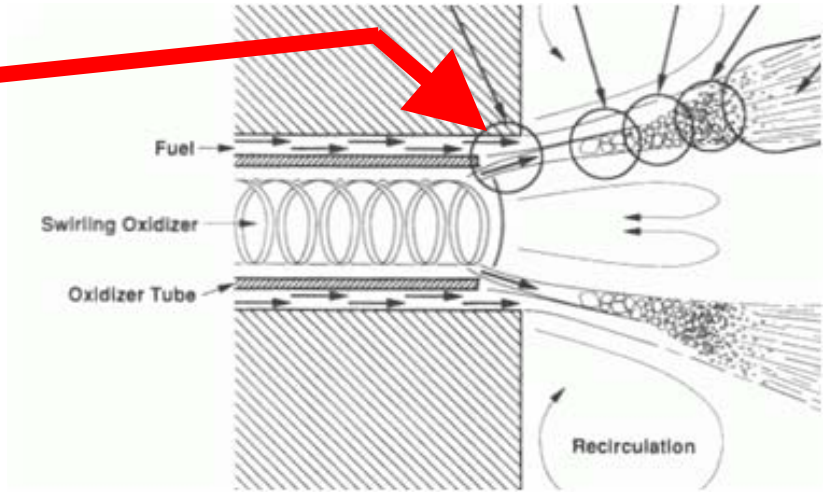


- For fuel *"d"* (with liquid methane) use annulus gap width
- For oxidizer *"d"* use swirl film thickness (from COBRA preburner presented in 2004 JANNAF)

# Hewitt Stability Correlation Predicts 1T Mode Instability with Oxidizer *"d"/V*

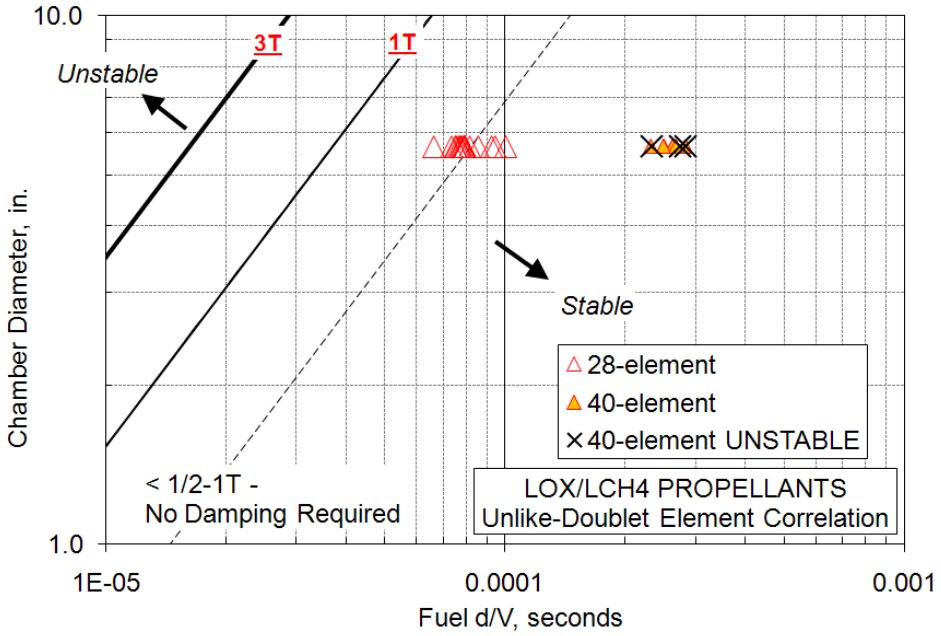


Fuel *d/V* based on
*d* ~ annulus gap flow

Oxidizer *d/V* based on
*d* ~ swirl film thickness

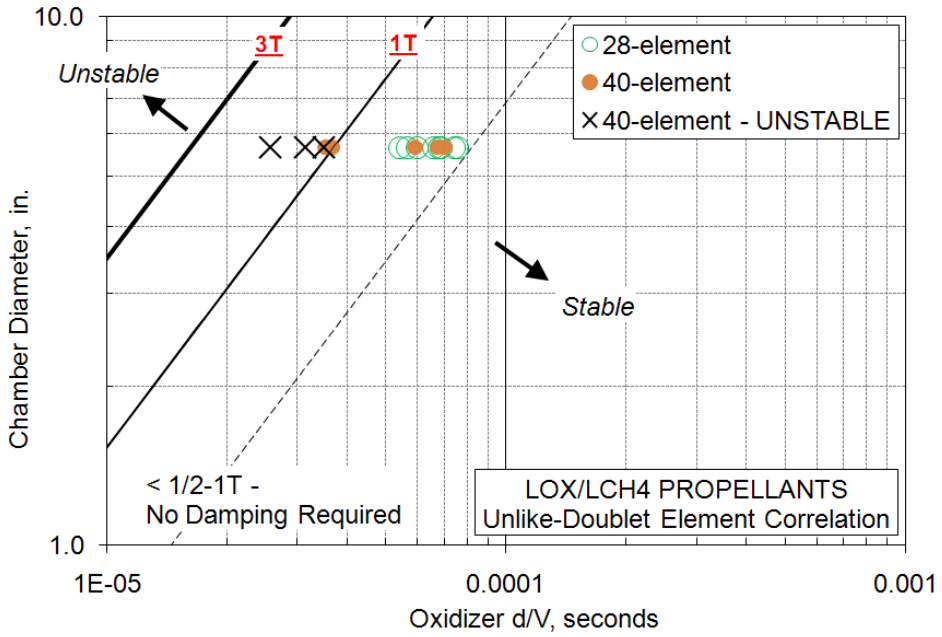

# Summary and Conclusions

- *a priori* performance predictions with 1-D codes with methane (and especially liquid methane) are not adequately reliable to support design of new combustion devices
  - Significant adjustments to atomization inputs for most cases
  - Predictions of liquid/gas shear coax ok at higher *Pc* but not at low *Pc*
  - Predictions with liquid/Liquid swirl coax show vaporization-limited combustion although with extensive user intervention
- Low-frequency combustion instability (chug )
  - Analysis models are adequate
  - Need further evaluation for why inlets broke on $LO_2/LCH_4$ swirl coax injector
- High-frequency combustion instability
  - Analysis of $LO_2/gCH_4$ shear coax element injectors focus on oxidizer post resonances
  - Analysis models for $LO_2/LCH_4$ swirl coax injectors need work
    - Oxidizer “gas core” resonances
      - Gas is combustion products
      - Tune it out or tune it in (“1T resonator” – Cha et.al, AIAA 2005-3748)
    - 1T mode instability driven by Hewitt *“d”/V* of oxidizer film thickness
      - Liquid oxygen side, not the liquid methane side
      - Previously observed during COBRA subscale preburner testing

# Recommendations

1) Extend the Burick shear coaxial element Rupe mixing correlation for methane (higher density) fuel.
2) Improve the atomization model for liquid methane injected from the outer annulus of a coaxial element.
3) Improve the atomization model for swirled liquid oxygen injected from the center orifice of a swirl coaxial element.
4) Generate atomization data (cold flow and hot-fire) for the liquid/liquid swirl coaxial element, including breakup length data and drop size data.
5) Develop new methods to calculate the atomization parameters for the CICM model.
6) Extend the tested range of conditions during hot-fire test programs, especially to lower chamber pressures, to generate a wider range of parametric data for validating model capability.

# Acknowledgements


- Funding provided by the NASA Glenn Research Center
  - Supervision by Mark Klem and Tim Smith
- Liquid/liquid multi-element injectors
  - Sandy Elam of NASA MSFC – design, fabrication, and test coordination
  - Cynthia Sprader of NASA MSFC – test conductor
- Ross Hewitt – Discussions on swirl coax stability